1. Introduction

1.1. Star formation process

The interstellar medium (ISM) is the matter (gas 99%, dust 1%) distributed in the space between the stars. Hydrogen (H) is the most abundant element of the ISM, and its physical/chemical state defines the ISM phases: the ionised phase, in which H is atomic ionised, the neutral phase, in which H is neutral atomic, and the molecular phase, in which H is neutral molecular (H_2). Star formation is the set of physical processes that forms stars from the material of the ISM. In particular, molecular clouds are the places where stars are born. The largest molecular clouds are called Giant Molecular Clouds (GMCs), with typical densities of 10^2–10^3 cm^{-3}, diameters greater than 25 pc, average temperatures of 10 K and masses of about 10^5 $M_\odot$ (e.g. Murray 2011). Turbulence, gravity and magnetic field give rise to dense cores of different mass and size through the fragmentation process inside a large GMC. Cores have typical sizes of 0.02–0.2 pc, masses of $\sim$0.5–5 $M_\odot$ and densities $>10^4$ cm^{-3} (e.g. Williams et al. 2000; Bergin and Tafalla 2007).

The standard theory of the formation of an isolated low-mass star[1] is based on the gravitational collapse of a single low-mass core (Shu et al. 1987; Shu 1991; Shu et al. 1993) through 3 main phases that are summarised in Fig. 1.1:

- A single core contracts quasi-statically and isothermally until it reaches an unstable configuration (*pre-stellar phase*). The time spent in this phase is $\sim 5\times10^6$ yr;

[1] Star with a mass similar to or lower than our Sun.

Laura Colzi, CAB - Astrobiology Center, Spain, lcolzi.astro@gmail.com, 0000-0001-8064-6394

FUP Best Practice in Scholarly Publishing (DOI 10.36253/fup_best_practice)

- The core can gravitationally collapse giving rise to a central protostar that accretes material from the parental cloud, and at the same time contracts onto itself becoming more and more dense and hot. If no other forces exist to oppose collapse, the core will collapse under its own gravity in a "free-fall time". This time is defined as:

$$t_{\rm ff} = \left(\frac{3\pi}{32G\rho}\right)^{1/2}, \tag{1.1}$$

  where ρ is the average mass density of the core. Magnetic field and turbulence are also important and provide additional support to cloud material against the gravitational collapse. Without entering into details (since it is not the subject of this thesis), if the core has a slight amount of initial rotation, the conservation of angular momentum during the collapse produces curved infall trajectories, giving rise to a disc-like structure. In this phase (*protostellar phase*), the protostar dissipates also a significant fraction of its angular momentum, into the surrounding environment, through bipolar outflows. The time of the accretion phase is $t_{\rm acc} = \frac{M_*}{\frac{dM}{dt}} \sim 10^5$ yr, where M_* is the protostellar mass and $\frac{dM}{dt}$ is the accretion rate of the gas to the center of the core;

- After the accretion is finished, the "naked" protostar goes on contracting (*pre-main sequence* or "*T-Tauri*" *phase*). The total contraction time of the protostar is the Kelvin-Helmholtz time, $t_{\rm K-H} = \frac{GM_*^2}{R_* L_*}$, where R_* is the protostellar radius and L_* is its luminosity. At the end of this time the star reaches an internal temperature that is sufficient to ignite hydrogen and hence to reach the Zero Age Main Sequence (ZAMS). The duration of this phase is $t_{\rm K-H} \sim 10^6$–10^7 yr.

1.1.1. The challenge of high-mass star formation

High-mass stars (or massive stars) have masses M>8M$_\odot$ and main sequence (MS) spectral types[2] from B3 to O2 (OB stars). Although massive stars make up less than 1% of the stellar population in the Milky Way (integrating the initial mass function by Kroupa 2001), they play a central role in many astrophysical processes, such as shaping the ISM, regulating star formation, and ultimately governing the evolution of their host galaxies (Kennicutt 2005). However, to date, understanding massive star formation remains a challenge.

The scenario presented above for the formation of low-mass stars is not applicable for massive stars. In fact, the standard theory cannot be applied to stars more massive than 8 M$_\odot$ because for these stars the accretion timescale is longer than the rapid Kelvin-Helmholtz, or contraction, timescale[3]. Therefore,

[2] Spectral types are identified by different letters (O, B, A, F, G, K and M) that are used to characterize stars according to their mass and temperature, from the most massive and hottest to the least massive and coldest.

[3] For a high-mass star the $t_{\rm KH} \sim 10^4$ yr is shorter than the $t_{\rm acc} \sim 10^5$ yr.

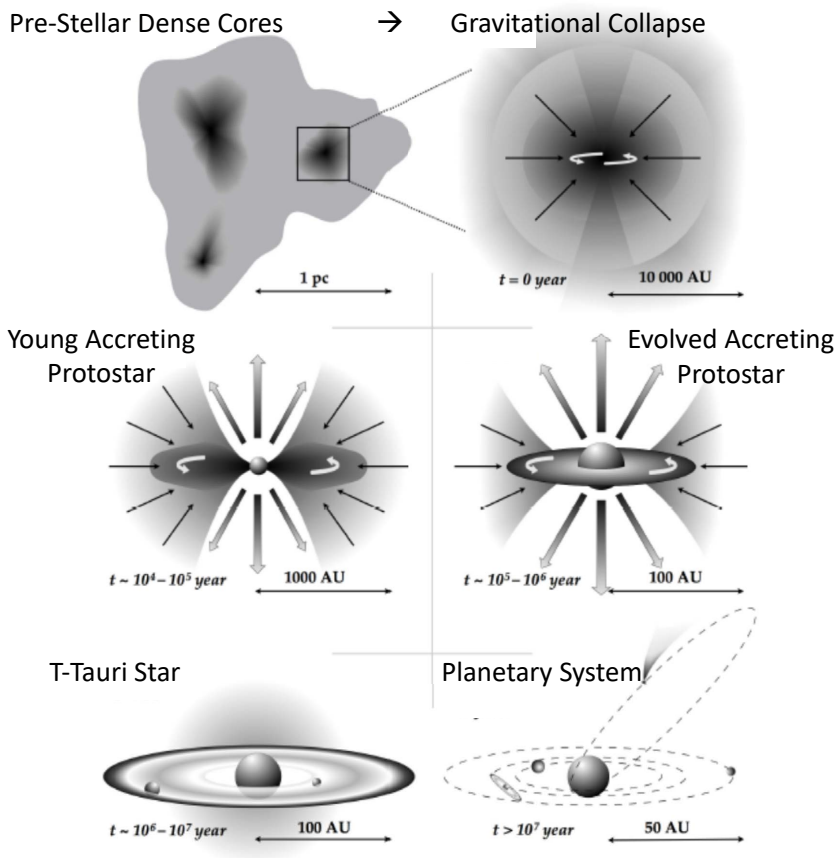

Fig. 1.1: Evolutionary stages for the formation of low-mass stars, adapted from Frieswijk (2008).

when the star arrives on the ZAMS, and the hydrogen starts to burn, the accretion from the surrounding gas continues. Then, a necessary condition to form a massive star (with mass M_*), is that the acceleration of a unit mass, dm, at a radius r, due to gravity, $\frac{GM_*}{r^2}$ must exceed the outward-directed radiative acceleration of the accreting gas, $\frac{\kappa L}{4\pi r^2 c}$. In the last expression κ is the opacity of the accretable material for ultraviolet (UV) radiation, L is the protostellar luminosity given by the sum of the intrinsic luminosity and the luminosity emitted from the dissipation of kinetic energy of the accreting material, and c is the speed of light. Therefore:

$$\frac{\kappa L}{4\pi r^2 c} < \frac{GM_*}{r^2}, \tag{1.2}$$

which translates into (Wolfire and Cassinelli 1987; Yorke 2004):

$$\kappa < \kappa_{\rm crit} = 130\ cm^2 g^{-1} \left[\frac{M_*}{10 M_\odot}\right] \left[\frac{L_*}{1000 L_\odot}\right]^{-1}. \quad (1.3)$$

Given typical values of the opacity of dusty ISM (κ $\sim$100 cm^2 g^{-1}), the Eq. (1.3) is not satisfied for MS stars more massive than $\sim$5 $M_\odot$ and luminosity of 10^4 $L_\odot$, for which $\kappa_{\rm crit} \sim 10$ cm^2 g^{-1}. With more refined models one finds that the limit at which Eq. (1.3) is satisfied is at about 8 $M_\odot$. Therefore, for such stars, the net force on dusty ISM is directed away from the star, and accretion cannot continue to allow the growth above 8 $M_\odot$. This effect is known as the radiation pressure problem.

Proposed solutions

To solve this problem at least one of these conditions must be satisfied:

- the radiative acceleration ($\propto$ L$_*$) must be reduced;
- the gravitational force ($\propto$ M$_*$) must be increased;
- the opacity of dusty ISM must be reduced.

In the last decade several works have shown that in theory is possible to overcome the radiation pressure problem and gather enough mass to build up a massive star. In the review of Tan et al. (2014), two main alternative theories are presented: the core accretion and the competitive accretion.

- *Core accretion*: it is a "scaled-up" version of low-mass star-formation (Fig. 1.1), characterised by higher accretion rates and non-spherical geometry. However, this scenario presents some problems as the theory assumes the existence of turbulent massive cores[4] that have prevented fragmentation during their formation. Radiative feedback from the star or magnetic fields are thought to inhibit fragmentation (e.g. Hosking and Whitworth 2004). However, several observations and simulations did not find turbulent massive condensations, but smaller and lower-mass fragmented objects (Pillai et al. 2011; Duarte-Cabral et al. 2013; Palau et al. 2013; Fontani et al. 2016; Fontani et al. 2018a), although a few recent massive starless core candidates possibly non-fragmenting have been proposed (e.g. Cyganowski et al. 2014; Nony et al. 2018).
- *Competitive accretion*: this theory relies on the fact that nearly all massive stars are formed in clusters together with low- and intermediate-mass stars (Lada and Lada 2003). Therefore, the stellar cluster environment may influence the massive star formation process. Numerical

[4] The typical sizes and masses of these objects are $\sim$0.2 pc and 100 M$_\odot$, respectively. Based on the size, in the literature sometimes they are called *clumps* rather than *cores*. Therefore, we note that although the nomenclature of this theory refers to the term *core*, their initial condensations are indeed *clumps*.

simulations have shown that the gravitational fragmentation of a molecular cloud produces fragments of gas and dust that collapse and form a low-mass star cluster (Bonnell et al. 2004). The overall potential well, created by the low-mass star cluster, funnels gas down to the potential center producing a global infall of material. Some of the stars accumulate the majority of gas and will become massive stars.

Testing the theories presented above with observations is challenging for several reasons: being at distances $\gtrsim$1 kpc massive star-forming regions have small angular sizes, they are few with respect to low-mass stars, and they are usually embedded in crowded environments (e.g. Zinnecker and Yorke 2007; Tan et al. 2019). Nevertheless, investigations of the natal environment of massive stars provide clues for a better understanding of its physical and chemical properties and of the star formation process itself.

Phases of massive star formation

For the reasons discussed above, for massive stars there is not an equivalent classification scheme like that described for low-mass stars (Fig. 1.1). Motte et al. (2018) introduce the most likely evolutionary scenario for high-mass star formation, which is summarised in Fig. 1.2. This scenario is based on observational constraints and follows the competitive/clump-fed scenario. The different phases that they propose are described as follow:

- 1. Massive stars form in molecular complexes hosting massive clouds and OB star clusters (i.e. where main sequence massive stars are already present). Parsec-scale clouds called ridges or hubs are the sites in which high-mass star-formation is preferred to occur. In particular, ridges are high-density filaments (n >10^5 cm^{-3}, diameter d of $\sim$5 pc) forming clusters of high-mass stars (e.g. Nguyen-Lu'o'ng et al. 2013), while hubs are more spherical and smaller clumps (d $\sim$1–3 pc), forming at most a couple of massive stars (e.g. Didelon et al. 2015).

- 2. Ridges are fragmented in IR-quiet massive dense cores (MDCs) of 0.1 pc (n>10^5 cm^{-3}, T<20 K), which host several low-mass pre-stellar cores. These objects are also considered as IR-dark clouds (IRDCs) since they do not emit strongly in the IR. IR-dark features are also seen in silhouette against the bright IR galactic background (e.g. Teyssier et al. 2002; Butler and Tan 2009), and are bright in the mm, with typical T$\sim$10–20 K and n$\gtrsim$$10^4$ cm^{-3} (e.g. Rathborne et al. 2006; Ragan et al. 2009).

- 3. The low-mass pre-stellar core accretes material from the parental clump. This accretion is generated by the global collapse of ridges that creates flow streams and increase the MDCs mass. This gas inflow accretes onto a high-mass protostar at MDCs centers.

- 4. After about 10^5 yr, on 0.01 pc scales, one massive protostar or a close binary system forms at the center of MDCs. Observationally, during the accretion, the low-mass protostellar cores become IR-quiet high-mass protostars. In this phase collimated jets and molecular outflows from the star might appear.

- 5. Then, high-mass protostars become IR-bright for stellar embryos larger than 8 $M_\odot$, which are similar to the low-mass protostellar objects but with higher densities and temperatures ($n \gtrsim 10^6$ cm^{-3}, $T \gtrsim 20$K).

- 6. Finally, when the hydrogen burning starts, the generated UV radiation ionises the surrounding hydrogen forming a hypercompact ($r \leq 0.01$ pc) HII region, that progressively expands to ultracompact HII regions (UC HII $r \leq 0.1$ pc) and finally becomes a classical HII region (1-10 pc).

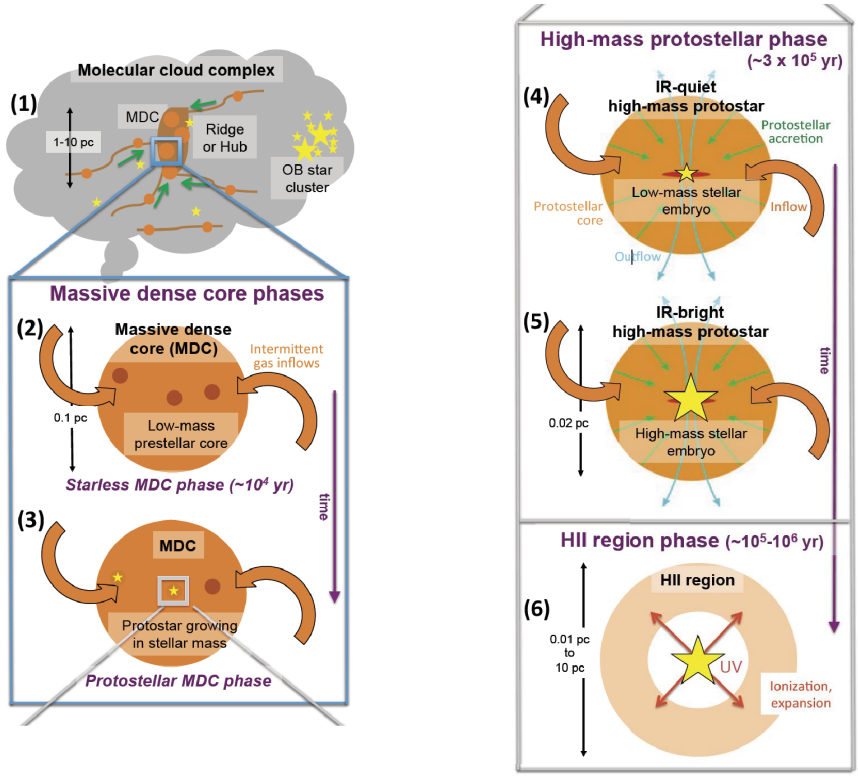

Fig. 1.2: Scheme of the evolutionary stages for the formation of massive stars, taken from Motte et al. (2018).

Gross evolutionary classification for massive star formation

Due to the short evolutionary timescales, and the possible overlaps between the processes described above, the phases presented in Fig. 1.2 can be divided empirically into three gross phases, as proposed by Beuther et al. (2007a):

- **High-Mass Starless Cores (HMSCs)**: these objects are in a phase immediately before the collapse or at an early stage of the collapse. HMSCs put together phases 2 and 3 of Fig. 1.2.

- **High-Mass Protostellar Objects (HMPOs)**: these are similar to the low-mass protostellar objects but with higher densities and temperatures ($n \gtrsim 10^6$ cm^{-3}, $T \gtrsim 20$K). In this phase collimated jets and molecular outflows from the star might appear. HMPOs put together phases 4 and 5.

- **UC HII regions**: these objects are already ZAMS stars still embedded in the natal cloud, and are part of phase 6 above. The pressure enhancement, due to the heating produced by the ionising radiation, produces an expansion of the hypercompact HII region, forming the so-called UC HII regions ($r \sim 0.1$ pc).

This classification, shown in Fig.1.3, is the one that has been used in this thesis, in particular in the works described in chapters 2 and 3.

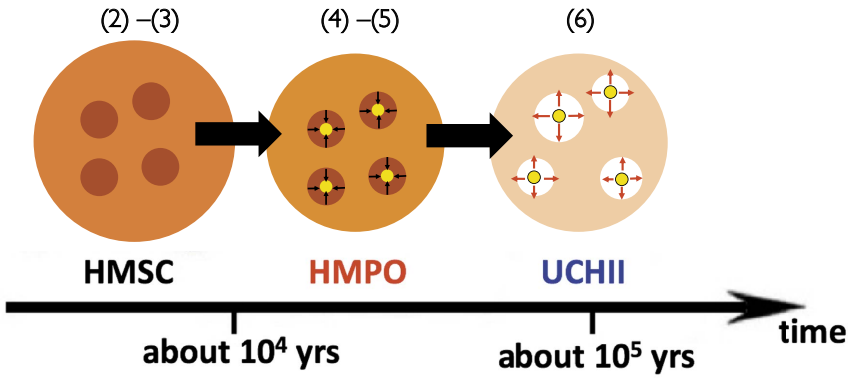

Fig. 1.3: Scheme of the gross evolutionary classification for high-mass star-forming regions, adapted from Beuther et al. (2007a). The numbers in the top represent the phases proposed by Motte et al. (2018) and described in the text.

1.2. The importance of high-mass star-forming regions for the Solar system formation

Nowadays, there is growing evidence that stars, including our Sun, do not form in isolation, but in rich clusters (e.g. Lada and Lada 2003). Adams (2010) discuss in his review the birth environment of the Sun from the extant properties of our Solar system. In particular, one of the physical processes that influenced the forming Solar system can be inferred by the presence of short-lived radioactive species in meteorites. Short-Lived Radionuclides (SLRs) are those with half-lives less than about 10 Myr. From the relative abundance of the daughter species in meteoritic samples it can be inferred how much time it takes from their production and their incorporation into the early Solar system. These measurements indicate that only a short time ($\sim$1 Myr) could have elapsed between the production of short-lived species and their subsequent incorporation into the early Solar system material. Supernova explosions provide one possible source of these radioisotopes. One example SLR is ^{26}Al, which has a half-life of 0.72 Myr and decaying creates ^{26}Mg, the amount of which is measurable in meteoritic samples. However, more recent works show that the ^{26}Al distribution in the early Solar system seems to have been heterogeneous (e.g. Liu et al. 2012). This suggests that the ^{26}Al is most likely produced from the wind of massive stars, and not from a single supernova explosion. Gounelle and Meynet (2012) proposed that ^{26}Al originated in a wind-shell around a massive star which, after several Myr, reaches large densities and becomes gravitationally unstable, giving rise to a second star generation. The presence of ^{26}Al in the early Solar system is also important to explain the bulk of the water that we expect during the formation of planetesimals. In fact, the decay heat from this SLR should have been sufficient to power the interior evolution of these bodies. Lichtenberg et al. (2019) use numerical models of planet formation to show that a planet's bulk water fraction is anti-correlated with initial ^{26}Al levels. The heat generated by the decay of this element rapidly dehydrates planetesimals before their accretion onto larger protoplanets. This would allow to form *dry* terrestrial planets like our Earth. Another SLR found in pristine Solar system material is the ^{60}Fe, the abundance of which could be explained only by the presence of, at least, two supernovae, as proposed by Portegies Zwart (2019). In fact, one is necessary to deliver the ^{60}Fe, and the other to preserve it in the proto-Solar disc.

Although some SLRs could be explained also by internal processes connected to the forming Sun itself (e.g. ^{10}Be, Gounelle et al. 2001), the processes mentioned above indicate that the forming Solar system was not in a peaceful, quiescent environment, but in the middle of a rich cluster including massive stars, some of which could have been exploded as supernovae. All of these arguments, thus, suggest that data from meteorites can be interpreted by both an external and internal enrichment mechanism into the early Solar system.

Another physical process that influenced the Solar system formation, discussed by Adams (2010), is the dynamics of the birth cluster that could have

affected stars and planets formation. In fact, the observed planetary orbits indicate that no passing stars have made disruptive encounters with the Solar system after the giant planets were formed. However, the orbit of the dwarf planet Sedna can be explained only with a close encounter, at a distance of 400-800 au. This information constrains the stellar density n_* of the Solar system birth environment, in residence time t in that region, to be of the order of $<n_*t>\sim$80000 pc^{-3} Myr. Since n_* $\sim$100 pc^{-3} is a mean typical stellar density, the Solar system must have lived in its birth cluster for a few hundred million years. In this case, only large bound clusters, with a number of membership $N>1000$ are expected to live that long (e.g. Kroupa 2001). The other possibility is that the Sun lived in a higher density environment.

The last point discussed by Adams (2010) is the possible external UV radiation field experienced by the young Sun, and provided by the cluster which could have played a role in shaping the proto-Solar nebula (PSN), in which our Sun was born. The far-UV (FUV) fluxes are expressed in units G_0, and G_0=1 corresponds to the flux in the solar neighbourhood $F_{\rm FUV}$=1.6$\times$10^{-3}erg s^{-1} cm^{-2} (Habing 1968). An external FUV with $G_0 \approx 10^4$ is necessary to photoevaporate the early Solar nebula beyond about 30 au and to explain the low amount of gas in ice giant planets, like Neptune and Uranus. This value is beyond the peak of the distribution for young clusters in the solar neighbourhood. This means that the birth cluster must be larger than the clusters in the neighbourhood of the Solar system, with N$\geq$1000.

A possible scenario that puts together these three points, for example, requires a cluster with at least N$\geq$1000, in order to produce a 25 M$_\odot$ star. This star could enrich the Solar system of the short-lived radioisotopes through its wind, and is able to explain both the possible external UV radiation G$_0$ $\leq 10^4$ and the present planet orbits (see Fig. 1.4).

Other evidence that our Sun was born in a cluster containing massive stars comes also from the works made by Taquet et al. (2016) and Drozdovskaya et al. (2018). In particular, Taquet et al. (2016) investigated the chemical and physical origin of O_2 using astrochemical models, and compared these results with the gas-phase O_2 recently observed in the coma of comet 67P/Churyumov-Gerasimenko (hereafter 67P, Bieler et al. 2015) by the *Rosetta* spacecraft. The main result that they obtained is that the molecular oxygen is mainly formed in dark clouds for higher densities ($\gtrsim 10^5$ cm^{-3}) and moderate temperatures ($\approx$20 K) with respect to those commonly considered as Solar system progenitor. In fact, this is the typical temperature of a high-mass starless core (HMSC, e.g. Fontani et al. 2011), and is hotter than that of isolated low-mass pre-stellar cores (<10 K, e.g. Keto and Caselli 2010). Furthermore, Drozdovskaya et al. (2018), searched for S-bearing species at a distance of 60 au from the proto-Sun analogous low-mass protostar IRAS 16293-2422 B (hereafter 16293B), and compared these results with data on comet 67P. They show that 16293B contains much more OCS than H_2S in comparison with 67P. A possible explanation is a a relatively warmer birth cloud of our Solar system, with respect to 16293B.

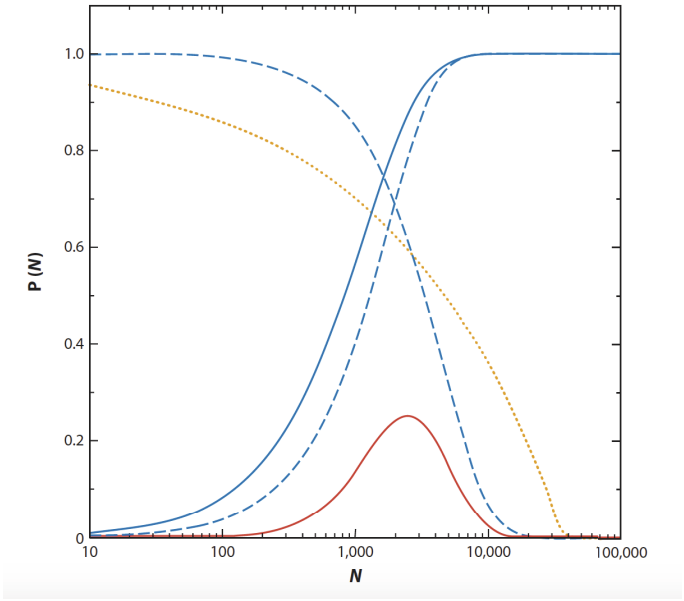

Fig. 1.4: Probability distributions for a cluster of membership size N as a function of N. In particular, the solid blue curve is the probability to produce a supernova with progenitor mass $M_* \geq 25$ $M_\odot$. The dashed blue curves represents the probability of a close encounter with a distance less than 400 au (to produce Sedna), but no encounters at a distance < 225 au in order to preserve the planetary orbits. The dotted orange curve is the probability to have an external FUV with $G_0 \leq 10^4$. Finally, the red solid line is the joint probability distribution with $<N> = 4300 \pm 2800$. Taken from Adams (2010).

In summary, the detailed study of the physical and chemical conditions of high-mass star-forming regions is important not only to understand the formation of massive stars, but also because they probably are the cradle in which our Solar system was born.

1.3. Astrochemical processes in the interstellar medium

Before discussing in detail the main topic of this thesis, let us briefly review the main processes that lead to the formation of molecules in the ISM. Molecules can form both on ice mantles of grains and through gas-phase reactions. In particular, in the gas phase, a chemical reaction can occur spontaneously if the variation of the Gibbs free energy, ΔG, is lower than zero. G is a state function used in thermodynamics that represents the free energy (U) of the isothermobaric reactions, i.e. those during which pressure (P) and temperature (T) remain constants. So, given that $G = H - TS$, with the enthalpy $H =$

$U + PV$ and the entropy S:

$$\Delta G = \Delta H - T\Delta S = \Delta U + R_{\rm g} T \Delta N + T\Delta S, \tag{1.4}$$

in which it is assumed a constant T during the reaction, and that the gas follows the ideal gas law $PV = \mathcal{N} R_{\rm g} T$ ($\mathcal{N}$ moles number, and $R_{\rm g}$ ideal gas constant). Considering that the typical temperatures in the ISM are low (∼10 K), the second and the third terms are negligible with respect to the first one. So, the condition to have $\Delta G \leq 0$ is $\Delta U \leq 0$, i.e. the internal energy of the reaction products must be less than the internal energy of the reactants. This means that the energy is transferred to the environment in which the reaction occurs (exothermic reaction).

During a reaction, before the formation of the products, there is an intermediate state in which some bonds are broken, but the final ones of the products are still not formed. In this state, the system possesses an amount of extra energy with respect to the rest internal energy of the reactants called "activation energy", because it is also the energy that needs to be provided to the reactants to activate the reaction (Fig. 1.5).

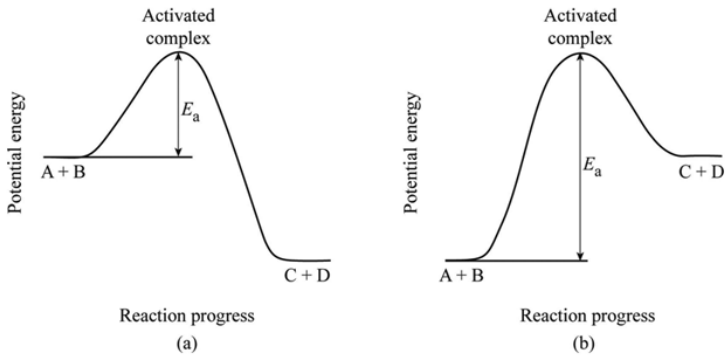

Fig. 1.5: Energy scheme of a reaction as a function of the reaction coordinate. Here the activation energy is noted by $E_{\rm a}$. *Left panel*: exothermic reaction. *Right panel*: endothermic reaction.

For example, in the reaction

$$\mathrm{C + H_2 \rightarrow CH + H}, \tag{1.5}$$

the H_2 bond energy is 4.48 eV, while that of CH is 3.47 eV: the reaction is endothermic (see right panel of Fig. 1.5), i.e. requires from the environment 1.01 eV to be spontaneous. Then, since 1 eV corresponds to $11.6{\times}10^4$ K, at the typical temperature of the ISM (10–100 K) this reaction is not spontaneous.

1.3.1. Gas-phase chemistry

Gas-phase reactions can be divided into different categories. Reactions such as photodissociation, dissociative recombination, and collisional dissociation are bond-destruction processes that fragment species into smaller ones. Other reaction types are, for example, ion-molecule reactions, charge-transfer reactions, and neutral-neutral reactions.

A general chemical reaction

$$\mathrm{A} + \mathrm{B} \xrightarrow{k} \mathrm{C} + \mathrm{D}, \tag{1.6}$$

is associated with his rate coefficient, k, which is a measure of the efficiency of the reaction. Generally, this coefficient is given in the form of a modified Arrhenius equation:

$$k = \alpha \left(\frac{T}{300\mathrm{K}} \right)^{\beta} \exp(\frac{-\gamma}{T}), \tag{1.7}$$

where β is a possible dependence on the temperature of the reaction and γ is the possible activation energy. This is a general formula used for most of the gas-phase reactions, but some reaction types are parametrized differently. We will discuss some of them later in this chapter and in chapter 5. k is also called capture-rate coefficient (k_{capture}), from the theory for barrierless reactions (e.g. Georgievskii and Klippenstein 2005). For a reaction like (1.6), the corresponding rates of formation and destruction of a species are

$$\frac{\mathrm{d}n(\mathrm{C})}{\mathrm{d}t} = kn(\mathrm{A})n(\mathrm{B}), \tag{1.8}$$

and

$$\frac{\mathrm{d}n(\mathrm{A})}{\mathrm{d}t} = -kn(\mathrm{A})n(\mathrm{B}), \tag{1.9}$$

respectively, where $n(i)$ is the number density of species i in cm^{-3}. The total rate of change in the number density of species X is thus given by

$$\frac{\mathrm{d}n(\mathrm{X})}{\mathrm{d}t} = \text{formation terms} + \text{destruction terms}. \tag{1.10}$$

For a reaction system with forward and reverse reactions,

$$\mathrm{A} + \mathrm{B} \underset{k_{\mathrm{r}}}{\overset{k_{\mathrm{f}}}{\rightleftharpoons}} \mathrm{C} + \mathrm{D}, \tag{1.11}$$

the equilibrium coefficient $K(T)$ is defined by the relation

$$K(T) = k_{\mathrm{f}}/k_{\mathrm{r}}, \tag{1.12}$$

where k_{f} and k_{r} are the forward and reverse rate coefficients, respectively.

The equilibrium coefficient $K(T)$ is defined by the equation (McQuarrie 1976):

$$K(T) = k_{\rm f}/k_{\rm r} = \left[\frac{m({\rm C})m({\rm D})}{m({\rm A})m({\rm B})}\right]^{3/2} \frac{q({\rm C})q({\rm D})}{q({\rm A})q({\rm B})} \exp(\Delta E_0/k_{\rm B}T), \tag{1.13}$$

where $m(...)$ are the masses of molecules, $q(...)$ are the internal molecular partition function, and ΔE_0 is the zero-point vibrational energy difference between the reactants and the products[5]. This latter is positive if the reaction is exothermic. Moreover, $k_{\rm B}$ is the Boltzmann constant, and T is the temperature. The partition functions are given by

$$q(T) = \sum_i g_i \exp(-E_i/k_{\rm B}T), \tag{1.14}$$

where g_i is the spin degeneracy of the level i and E_i is the energy of the ith state. If there is no coupling, the partition functions can be factored in the three therms corresponding to the electronic, vibrational and rotational-nuclear spin terms.

A simplified expression for $K(T)$, equivalent to (1.13), is

$$K(T) = f(B, m) \exp(\Delta E_0/k_{\rm B}T), \tag{1.15}$$

in which the factor f is called "symmetry factor" and depends on the rotational constants, B, of molecules involved in the reaction, masses and symmetries of the reactants and products (e.g. Terzieva and Herbst 2000).

1.3.2. Type of reactions

Two of the main type of reactions that could occur in the ISM are the neutral-neutral and the ion-neutral ones (e.g. Tielens 2005). The property that distinguishes them is the rate of two-body collisions, $k_{\rm AB}$. If particles B are characterised by a velocity distribution relative to particles A, $f({\rm v})$, then

$$k_{\rm AB} = \int_0^\infty {\rm v} f({\rm v}) \sigma_{\rm AB}({\rm v})\, d{\rm v} \quad {\rm cm^3 s^{-1}}, \tag{1.16}$$

where $\sigma_{\rm AB}({\rm v})$ is the collisional cross-section. If particles B follow the Boltzmann energy distribution, then the velocity distribution is the Maxwell one:

$$f({\rm v}) = 4\pi {\rm v}^2 \left(\frac{\mu}{2\pi k_{\rm B}T}\right)^{\frac{3}{2}} \exp\left(-\frac{\mu {\rm v}^2}{2k_{\rm B}T}\right), \tag{1.17}$$

[5] The zero-point energy (ZPE) is the lowest possible energy that a quantum mechanical system may have. In our case, the systems are the single molecules, and their ZPE is defined as the lowest quantum energy level.

where T is the gas kinetic temperature, μ is the reduced mass of the reactants, and v is the relative velocity. Thus, substituting in eq. (1.16),

$$k_{\rm AB} = 4\pi\left(\frac{\mu}{2\pi k_{\rm B}T}\right)^{\frac{3}{2}}\int_0^\infty {\rm v}^3\exp\left(-\frac{\mu {\rm v}^2}{2k_{\rm B}T}\right)\sigma_{\rm AB}({\rm v})\,d{\rm v}. \tag{1.18}$$

For different reactions, $\sigma_{\rm AB}$, and hence $k_{\rm AB}$, is different:

- **neutral-neutral reactions**: the collision of the two particles can be approximated as that of two rigid spheres. In this case the cross-section is given by the geometric area defined by the distance between the sphere centres, $\sigma_{\rm AB} = \pi(r_{\rm A} + r_{\rm B})^2$, and then taking A = B = hydrogen with mass $m_{\rm H}$, equation (1.18) becomes:

$$k_{\rm AB} = 1.81\times10^{-10}\left(\frac{T}{10^2{\rm K}}\right)^{\frac{1}{2}}\left(\frac{m_{\rm H}}{\mu}\right)^{\frac{1}{2}}\left(\frac{r_{\rm A}+r_{\rm B}}{2\,\text{Å}}\right)^2 \quad {\rm cm^3 s^{-1}}; \tag{1.19}$$

- **ion-neutral reactions**: in this case the spherical approximation is not valid. The two particles react also at large distance through the electrostatic attraction between the ion and the dipole moment induced on the neutral particle. The cross section could be described by $\sigma_{AB} = \pi b_0^2$, where b_0 is the limit cross distance, beyond which there is no collision (Duley and Williams 1984). One can demonstrate that b_0 is a function of the polarizability of the neutral species, α, and then (1.18) becomes:

$$k_{\rm AB} = 2.34\times10^{-09} q\left(\frac{\alpha}{\mu}\right)^{\frac{1}{2}} \quad {\rm cm^3 s^{-1}}, \tag{1.20}$$

where α is in cubic angstroms, μ is in atomic mass units (amu), and q is the electronic charge in unit of 4.80×10^{-10} esu, that is the c.g.s. expression for the elementary charge. This rate coefficient is also called "Langevin rate", $k_{\rm L}$ (e.g. Tielens 2005), and to a first approximation it is independent on the temperature. At high temperatures, the rapid rotation of neutral species over various directions generate an average value of zero for the dipole moment. However, the latter is not zero at low temperatures since neutral species rotate slowly. Complex dependences on the temperature have been proposed and, for example, for ion-neutral reactions with a dipole moment it can be used the Su-Chesnavich capture approach (e.g. Woon and Herbst 2009 and Wakelam et al. 2012). In particular, the rate for these reactions is expressed in terms of the Langevin rate using two formulas, one for lower and one for higher temperatures. The temperature ranges will depend on the parameter x, defined as:

$$x = \frac{\mu_{\rm D}}{\sqrt{2\alpha k_{\rm B}T}}, \tag{1.21}$$

where μ_D is the dipole moment in units of Debye (1 D = 10^{-18} statC cm). The rate coefficient is then expressed as follows:

$$k_{AB} = \alpha k_L \left(0.62 + 0.4767\gamma \left(\frac{300}{T}\right)^{1/2}\right) \quad \text{if } x \geq 2, \tag{1.22}$$

$$k_{AB} = \alpha k_L \left(1 + 0.0967\gamma \left(\frac{300}{T}\right)^{1/2} + \frac{\gamma^2}{10.526}\frac{300}{T}\right) \quad \text{if } x < 2, \tag{1.23}$$

where α, in this case, is the branching ratio of the reaction, while γ represents the value of x at 300 K.

From what described above, at low temperature the ion-neutral reaction k_{AB} is constant (because temperature-independent), while for neutral-neutral reactions decreases. This is the reason why ion-neutral reactions are the most probable to occur in the molecular clouds, where often temperature is as low as 10 K.

Basics of carbon, oxygen, and nitrogen chemistry

The most abundant molecular ion of the ISM is H_3^+, formed by the following reactions:

$$H_2 + \text{c.r.} \rightarrow H_2^+ + e^- + \text{c.r.}, \tag{1.24}$$

and

$$H_2^+ + H_2 \rightarrow H_3^+ + H. \tag{1.25}$$

This very abundant ion triggers many ion-neutral reactions. In fact, it can easily donate a proton and allows the formation of bigger and bigger molecules.

For example, oxygen (O) chemistry starts from reactions shown in Fig. 1.6, and in particular with a proton transfer from H_3^+ to the neutral oxygen. Oxygen leads to the formation of water, H_2O, a molecule important for life on Earth. The formation of organic molecules and hydrocarbons from atomic carbon follows a similar path (see the bottom-right panel in Fig. 1.6), starting from neutral atomic carbon that reacts with H_3^+. Note that in diffuse clouds the OH^+ and CH^+ ions can also form starting from O^+ (that forms from O + H^+) and C^+ (that is the dominant form of carbon in diffuse clouds), respectively. In fact, the O^+ and C^+ ions react with H_2 forming OH^+ and CH^+ (for more details see Yamamoto 2017). However, nitrogen (N) chemistry do not start with the reaction

$$N + H_3^+ \rightarrow NH^+ + H_2, \tag{1.26}$$

given that it is endothermic. This chemical network starts with the neutral-neutral reaction

$$CH + N \rightarrow CN + H, \tag{1.27}$$

and can form molecules such as HCN, N_2H^+ or NH_3 (Fig. 1.6).

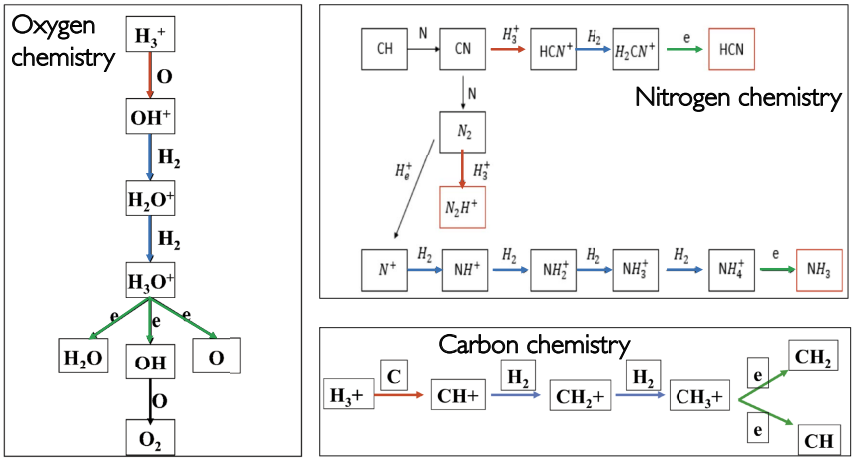

Fig. 1.6: Carbon, nitrogen, and oxygen chemical networks. The red arrows represent the proton transfer reactions, the blue arrows represent the hydrogen abstraction reactions, and the green arrows are the dissociative recombination reactions with electrons. Adapted from Duley and Williams (1984).

1.4. Isotopic fractionation in the context of star formation

Isotopic fractionation is the set of processes that distributes different isotopes[6] of an element in molecular species. The study of the isotopic fractionation during the different phases of star formation is a powerful tool to understand how the chemical content can be transferred from the initial molecular clouds to planetary systems. However, the processes by which it proceeds during star formation are not well understood and are a highly debated topic in the astrochemistry field. In this section the state-of-the-art of isotopic fractionation of hydrogen and nitrogen, and their link with the chemical complexity at different phases of star formation, is presented.

1.4.1. The evolution of chemical complexity during star formation

Chemical complexity in low-mass star-forming regions

Star formation and molecular complexity evolve closely together. In fact, a rich chemistry has been observed during the different phases of star formation (Fig. 1.7). Recalling the main phases of Sun-like star formation, they can be described also from a chemical point of view (Caselli and Ceccarelli 2012):

- **Pre-stellar cores.** At the low temperatures (∼10 K) of this phase, the gas-phase chemistry is dominated by ion-neutral reactions, as discussed in

[6] Isotopes are variant of a chemical element which differ in the number of neutrons.

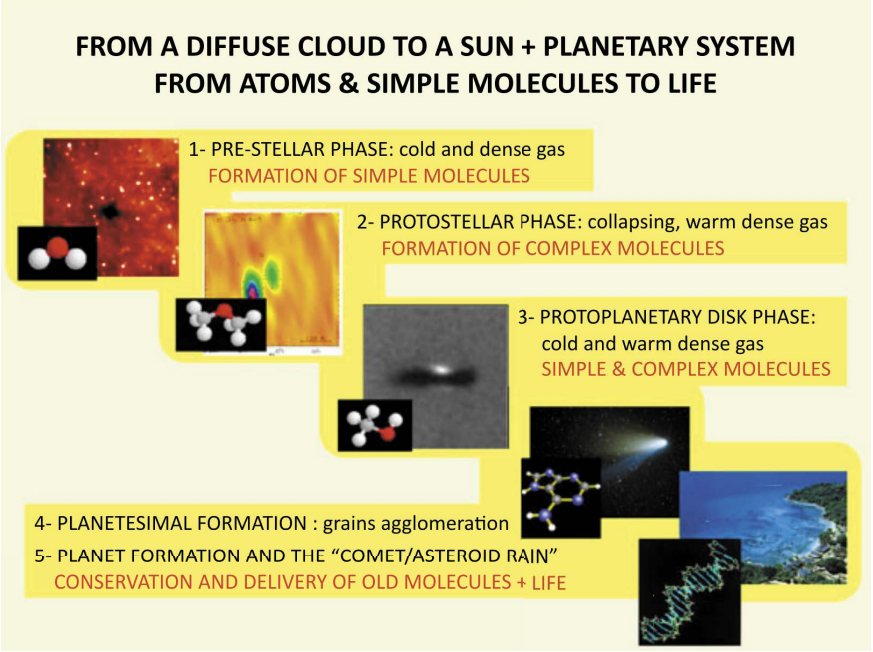

Fig. 1.7: Simplistic view of the evolution of chemical complexity, hand in hand with phases of Sun-like star formation. Taken from Caselli and Ceccarelli (2012).

Sect. 1.3. Atoms and molecules can directly react in gas-phase, and if the gas temperature allows to overcome the activation energies of exothermic reactions, more complex chemistry progresses. Moreover, if the density is high enough ($\geq 10^6 cm^{-3}$) and the temperature is $\leq$10 K, molecules and atoms in the gas-phase freeze-out[7] onto the cold surfaces of sub-micron size dust grains. H atoms have high mobility on dust surfaces, and this allows the hydrogenation of atoms and CO (the molecule most abundant in the ISM, after H_2). In this way molecules such as water (H_2O), formaldehyde (H_2CO) and methanol (CH_3OH) can be formed efficiently on the surface of dust grains. It has been observed that also more complex organic molecules (e.g. CH_3OCH_3) are already formed in these initial phases of star formation (e.g. Bacmann et al. 2012; Vastel et al. 2014; Jiménez-Serra et al. 2016).

- **Protostellar envelopes.** In this phase the temperature increases and when the envelope reaches the mantle sublimation temperature, the molecules formed onto ice surfaces sublimate. Here they can react and form more complex molecules. Moreover, collimated jets and molecular outflows are present and, when impacting the quiescent gas of the birth molecular

[7] The adsorption of species onto dust grain surfaces.

cloud, create shocks that partially sputter the ice mantles and refractory materials of grains, injecting molecules into the gas phase.

- **Protoplanetary discs.** In the colder inner substrates of the disc, molecules formed during the protostellar phase freeze-out onto ice mantles, and could still preserve a part of the composition of the pre-stellar phase. The process of "conservation and heritage" begins.
- **Planetesimal formation.** While the grains glue together forming pebbles and planetesimals, part of the icy grain mantles is preserved. Thus, part of the chemical history of the first phases of star formation is conserved in the building blocks of the Solar System rocky bodies.
- **Planet formation and the comet/asteroid rain.** Comets and asteroids that arrive onto the primitive Earth also release the heritage conserved in the ice trapped in planetesimals and rocks.

Chemical complexity in high-mass star-forming regions

In high-mass star-forming regions the chemistry evolves similarly to the low-mass star-forming ones. Recalling the three main evolutionary stages described in Sect. 1.1.1 and Fig. 1.3, the chemical evolution could be described as follows (e.g. Bisschop et al. 2007; Beuther et al. 2009):

- **HMSCs**: mostly simple molecules (like CO, N_2H^+, HCN, HNC, CN) form during this phase, as in the low-mass case. Moreover, the chemical complexity grows on dust grains thanks to the freeze out of molecules into ice mantles. Most saturated and complex species, such as H_2CO, CH_3OH, C_2H_5OH, $HCOOCH_3$, and CH_3OCH_3, probably result from a "first generation" chemistry in ices, likely dominated by surface chemistry.
- **HMPOs**: some of the species formed in ice mantles desorb thanks to the higher temperatures (>20 K) during this phase. Moreover, extended outflows and shocks sputter the mantles and refractory materials of grains directly in the gas phase. These objects are also characterised by H_2O and methanol masers (e.g. Moscadelli et al. 2017; Sanna et al. 2018);
- **UCHIIs**: this phase is characterised by ionised hydrogen (H^+), and a high electronic density ($n_e \geq 10^4$ cm^{-3}). These regions are traced, for example, by the free-free radiation (or thermal bremsstrahlung) at cm wavelengths. Moreover, the central envelope is chemically enriched as the HMPO phase (e.g. Bisschop et al. 2007; Fontani et al. 2007).

1.4.2. The heritage of the Solar system

A powerful tool to understand the chemical heritage from the earliest to the latest phases of the Solar system formation is the study of isotopic anomalies,

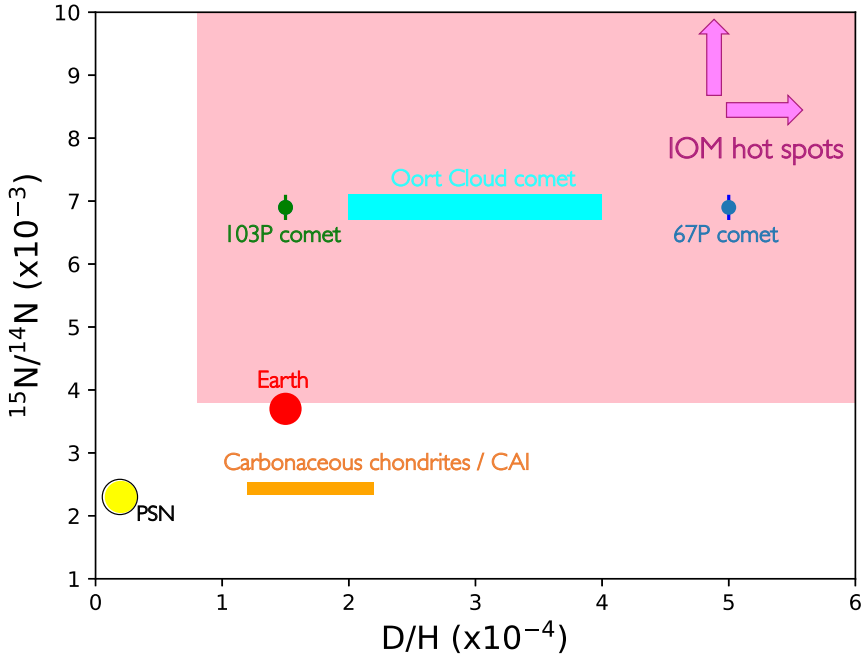

Fig. 1.8: $^{15}N/^{14}N$ vs D/H in comets, chondrites, hot spots in the IOM of meteorites, Earth and PSN.

in particular those measured for D/H and $^{14}N/^{15}N$. In fact, the isotopic values of hydrogen, nitrogen and oxygen derived for the proto-Solar nebula differ by a factor of ∼2 with respect to those measured in comets and carbonaceous chondrites[8], which represent the pristine Solar system material. This indicates that the isotopic values have been altered due to physical/chemical processes during the formation of the Sun. Isotopic anomalies could also give important information about the Galactic environment in which our Sun was born. For example, the anomalous $^{18}O/^{17}O$ in meteorites (5.2±0.2, Wouterloot et al. 2008) with respect to the Galactic value (4.1±0.1, Young et al. 2011) is another proof of injection of material from a type II supernova exploded near the Solar system just before its birth.

In this thesis I will focus on the isotopic fractionation of nitrogen, hydrogen, and carbon in star-forming regions.

[8] They are a class of chondritic meteorites and include some of the most primitive material. Chondritic meteorites are stony meteorites that have not been modified due to the melting or differentiation of the parent body.

Deuterium in pristine materials

The D/H ratio for the PSN was estimated to be $(2.1\pm0.5)\times10^{-5}$ (Geiss and Gloeckler 1998). Different values of the D/H ratio have been estimated in comets: in the Jupiter-family comet 67P, the D/H ratio measured in H_2O is about 5×10^{-4} (Altwegg et al. 2015), approximately three times that of Earth's oceans (1.5×10^{-4}). However, results from *Herschel* have shown D/H$\sim1.5\times10^{-4}$ in another Jupiter-family comet, 103P/Hartley (Hartogh et al. 2011), which is the same as in the Earth oceans. Other measurements are from the Oort Cloud comets, where the HDO/H_2O ratio has been measured to be $\sim3\times10^{-4}$ in C/1996 B2 (Bockelée-Morvan et al. 1998), $\sim4\times10^{-4}$ in 8P/Tuttle (Villanueva et al. 2009), and in C/2009 P1 it is 2×10^{-4} (Bockelée-Morvan et al. 2012).

Deuterium enrichment in Earth's oceans with respect to the PSN value has been investigated and two theories were proposed. The first theory suggested that water is delivered to Earth from comets during the Late Heavy Bombardment (Gomes et al. 2005). This theory was encouraged by the *Herschel* measurement toward the comet 103P/Hartley that presents the same H/D value than that of the terrestrial oceans. The second theory is based on the possibility that the Earth was partly built from water-rich planetesimal from the outer zone (Morbidelli et al. 2000). The HDO/H_2O measured in carbonaceous chondrites is in agreement with this theory (see Fig. 1.8).

Deuterium enrichment has also been observed in HCN, in the comet C/1995 O1 (Meier et al. 1998), and it is 10 times larger than the water D-enrichment. This difference is one of the hints that different chemical formation pathways could occur for the two different species.

In carbonaceous chondrites, values of D/H$\sim$1.2-2.2$\times10^{-4}$ in hydrous silicates were obtained (Robert 2003), and are very similar to that of the terrestrial oceans. Furthermore, very high D/H ratios of $\sim10^{-2}$ have been found in small regions in insoluble organic matter (IOM) of meteorites (Remusat et al. 2009); these regions are called "hot spots". In addition, interplanetary dust particles (IDPs) presents very variable values, from D/H$\sim8\times10^{-5}$ up to $\sim10^{-2}$. The values described above are shown in Fig. 1.8.

^{15}N in pristine materials

The $^{14}N/^{15}N$ ratio measured for the PSN is about 441 (Marty et al. 2010). A $^{14}N/^{15}N$ ratio of 139±26, from HCN, was estimated in the comet 17P/Holmes after an outburst (Bockelée-Morvan et al. 2008). Manfroid et al. (2009) estimated a mean value of $^{14}N/^{15}N$=148±6 from CN in 18 comets. Fig. 1.9 summarises $^{14}N/^{15}N$ measured in comets from HCN, CN, and NH_2. The values found in different comets are similar, with an average value of $^{14}N/^{15}N$=144±3.

Different values of $^{14}N/^{15}N$ were estimated in the carbonaceous chondrite Isheyevo: $\sim$424 in an osbornite-bearing calcium-aluminium-rich inclusion (CAI) (Meibom et al. 2007), and from 44 up to 264 (van Kooten et al. 2017)

in lithic clasts. In the latter the maximum value is similar to the typical one derived in the terrestrial atmosphere (TA), as derived from N_2, ∼272 (Marty et al. 2009). The ^{15}N-enrichment in the terrestrial atmosphere, as well as that in other rocky planet atmospheres (e.g. Mars), is still not well understood. This value could be linked to the history of asteroids fallen to the Earth, or to a secondary atmospheric processing (Marty et al. 2009). Measurements in carbonaceous chondrites are made in specific parts of the objects, as described above, while measurements in comets refer to average values in cometary comae. For these reasons, the values obtained from extraterrestrial material studied on Earth could be different from observations of comets. At the same time, different values from different parts of the same chondrite are measured, and this indicates that different parts of a chondrite are formed during different times of star formation. Meibom et al. (2007) infer that the carbon-bearing titanium-nitride (osbornite) in the Isheyevo CAI formed by gas-solid condensation, started in a high-temperature (∼2000 K) inner region (<0.1 AU) of the PSN, where all solids were initially evaporated and the gas homogenized. Under such high-temperature conditions, little isotopic fractionation is expected between gas and solids, and the nitrogen isotopic composition of osbornite in the Isheyevo CAI must be representative of the Solar nebula. In fact, winds associated with bipolar outflows, or turbulent transport of the hot inner nebula (silicate) dust, may have carried small refractory particles out to colder zones where CAIs were incorporated during protoplanet formation. van Kooten et al. (2017) infer, from isotope data of Isheyevo lithic clasts, that these variations in N isotopes are consistent with the accretion of multiple organic precursors and subsequent alteration by fluids with different (isotopic) compositions, taking place in more evolved stages of protoplanetary formation than the enrichments in CAI.

All of these values are different than those measured for the PSN, as summarised in Fig. 1.8, suggesting that at some point of the Sun formation D- and ^{15}N-enrichment processes occurred. One possibility is a direct heritage of the chemical complexity from the pre-stellar core phase or the protoplanetary disc phase. For this reason observations of H- and N-fractionation in these phases are really important to understand D- and ^{15}N-enrichments in pristine Solar system materials, and also in our Earth.

1.4.3. Deuterium enrichment during star formation

How the D/H ratio changes in different phases of star formation in the ISM was highly debated in past years. Nowadays there is a common opinion on the main process that enhances or decreases deuterium in molecules in molecular clouds. In this section the general idea, based both on theoretical and observational results, is reviewed.

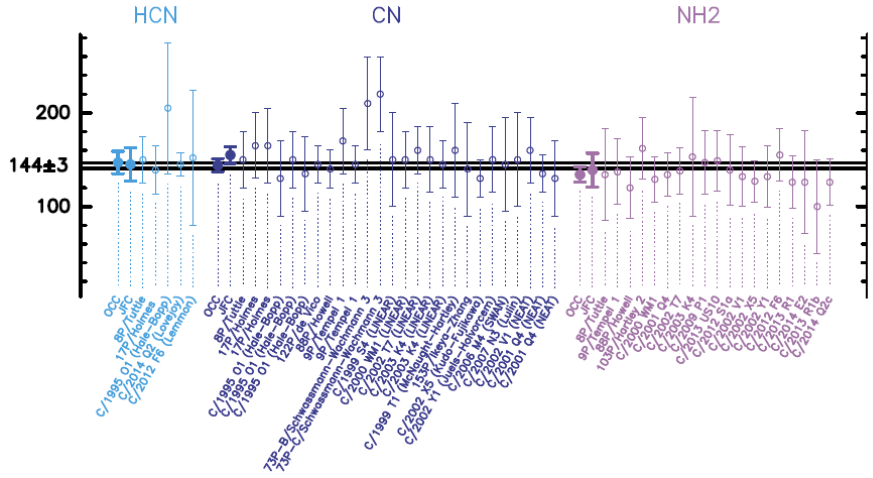

Fig. 1.9: Compilation of all $^{14}N/^{15}N$ ratios measured in comets. Taken from Hily-Blant et al. (2017).

D-fractionation in low-mass star-forming regions

Low-mass pre-stellar cores present densities that go from $\sim 10^3$ cm^{-3} in the outer part, to about $\sim 10^7$ cm^{-3} in the inner 1000 au[9]. Between 7000 and 15000 au the gas density is about 10^4 cm^{-3} and the temperature $\sim$10 K. In this region classical dark-cloud chemistry is at work with a high probability of ion-molecule reactions that dominate the carbon chemistry and create CO. Less important but probable are also neutral-neutral reactions that start the transformation of nitrogen atoms into nitrogen-bearing molecules, N_2, N_2H^+, and NH_3. First carbon and nitrogen chemistry are summarised in Fig. 1.6. Moreover, in the inner 7000 au the density increases to $\sim 10^5$ cm^{-3} and the temperature drops below 10 K. In these regions carbon-bearing species like CO, tend to disappear from the gas-phase and to be adsorbed onto dust grain surfaces. Freeze-out is a consequence of both low temperature and high-density environments. In fact, thanks to the high densities ($\sim 10^5$ cm^{-3}) there is a high probability that gas particles impact on dust grains. Thus, once species land on grain surfaces, they cannot thermally evaporate since their binding energies, E_B, are higher than 1000 K and the thermal evaporation rate is $\propto \exp[-E_B/k_BT]$. However, there is the possibility that a small fraction of the adsorbed species can return in the gas-phase via desorption caused by cosmic-rays impact into the grain surface, or photodesorption due to the FUV field

[9] These values of density and distance refer to those derived by Keto and Caselli (2010) for the pre-stellar core L1544. We note that this might not apply for other low-mass star-forming regions, even thought the general structure is likely to be similar.

produced by cosmic-ray impacts with H_2 molecules.

In the dense and low-temperature environment of pre-stellar cores, where ion-molecule reactions are favoured, chemical fractionation occurs, as described by Herbst (2003) starting from the reactions:

$$H_3^+ + HD \rightleftharpoons H_2D^+ + H_2 + 232K, \tag{1.28}$$

$$CH_3^+ + HD \rightleftharpoons CH_2D^+ + H_2 + 390K, \tag{1.29}$$

$$C_2H_2^+ + HD \rightleftharpoons C_2HD^+ + H_2 + 550K. \tag{1.30}$$

These reactions are called isotopic-exchange reactions and are caused by a thermodynamic effect in which the reaction has a preferred direction owing to exothermicity caused by a difference in the zero point energies between reactants and products. Reaction (1.28) produces an enhanced H_2D^+/H_3^+ abundance ratio for temperatures lower than $\sim$20 K (since the reaction from right to left is very inefficient) and when H_2 is mainly in the para form (anti-parallel H spins, e.g. Pagani et al. 1992; Walmsley et al. 2004). Moreover, in dense cores CO freezes out onto dust grains (e.g. Caselli et al. 1999). Since reaction with CO is the main destruction pathway of H_3^+ and H_2D^+, these two species remain abundant. Then, the high H_2D^+/H_3^+ is propagated to other molecules that react with the two ions. The grain surface chemistry on icy material during the early cold phase is also expected to play an important role for the deuteration of neutral species such as water (H_2O), formaldehyde (H_2CO), methanol (CH_3OH), and complex organic molecules (e.g. Cazaux et al. 2011; Taquet et al. 2012; Chacón-Tanarro et al. 2019). The reason is that the enhanced abundances of the deuterated forms of H_3^+ (H_2D^+, D_2H^+, D_3^+) produce enhanced abundances of D atoms in the gas-phase upon their dissociative recombination with electrons. The enhanced D abundance causes D/H ratio up to $\sim$0.1, so that molecules on the surface of dust grains (in particular CO) can be deuterated, to produce singly and doubly deuterated water and formaldehyde as well as singly, doubly, and triply deuterated methanol (e.g. Caselli and Ceccarelli 2012; Ceccarelli et al. 2014).

From an observational point of view, as a proof of the importance of reactions (1.28), (1.29) and (1.30), the ground state line of *ortho*-H_2D^+ was detected towards the starless core L1544 in the Taurus Molecular Cloud by Caselli et al. (2003). Fig. 1.10 shows the continuum map of this pre-stellar core, and the inner densest part is the one in which the deuteration of molecules occurs as explained above. Moreover, Vastel et al. (2004) detected the D_2H^+ ion in LDN 1689N, providing strong observational support for the D-fractionation theory.

Roueff et al. (2005) presented a steady-state model of the gas-phase chemistry for pre-stellar cores, including passive depletion on dust grains and multiply deuterated species. They compared the results of this model with observations of NH_2D, ND_2H, and ND_3 towards 5 pre-stellar cores. They obtained

ND_3/NH_3 ratios between 2×10^{-4} and $1–2\times10^{-3}$, which imply an enhancement factor of 11–12 order of magnitude over the cosmic D/H value. Their model predicts that high densities and high C and O depletion yield to an enhancement of the relative abundance of deuterated ammonia isotopologues, in agreement with observations (see also Gerin et al. 2006).

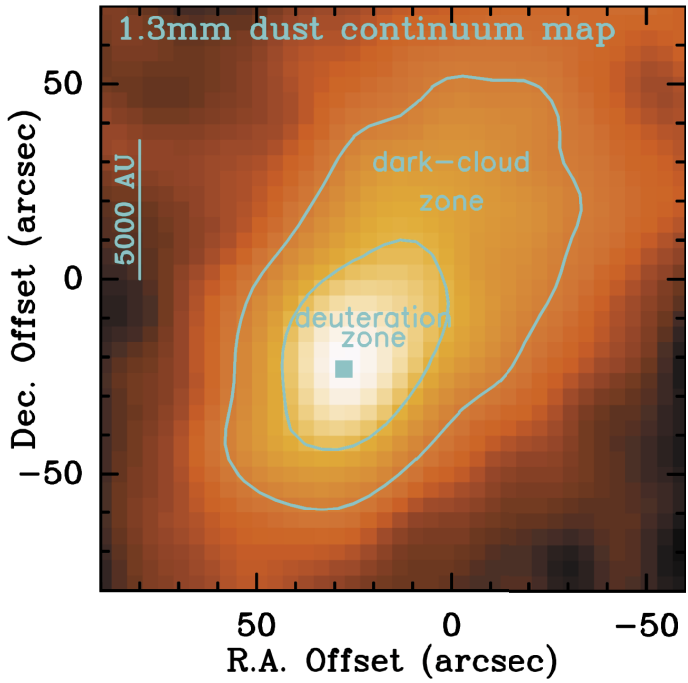

Fig. 1.10: The color scale represents the 1.3 mm dust continuum emission map obtained with the IRAM 30m radiotelescope by Ward-Thompson et al. (1999) towards the pre-stellar core L1544. Cyan contours indicate the two zones in which chemistry could be divided: the inner part is the one in which deuteration of molecules is enhanced. Image taken from Caselli and Ceccarelli (2012).

Crapsi et al. (2005) observed N_2H^+ and N_2D^+ towards a sample of 31 low-mass starless cores finding that the $N(N_2D^+)/N(N_2H^+)$ ratio is larger in the cores closest to the gravitational collapse. Emprechtinger et al. (2009) found also that $N(N_2D^+)/N(N_2H^+)$ ratio could be used as an evolutionary tracer for young protostars still embedded in their cold envelope. They derived that $D_{\rm frac}(N_2H^+)=N(N_2D^+)/N(N_2H^+)$ decreases with the protostar evolution. Moreover, Caselli et al. (2008) found, from observations of a sample of 10 starless cores and 6 protostellar cores, that the *ortho*-H_2D^+ is on average more abundant towards the starless cores than in the protostellar sources.

Recently, Redaelli et al. (2019) performed a detailed non-local thermodynamic equilibrium (non-LTE) analysis of N_2H^+, N_2D^+, $HC^{18}O^+$, and DCO^+

across the whole L1544 core. They found that N_2H^+ is more deuterated than HCO^+ (D/H=26% and 3.5%, respectively), as a consequence of the fact that N_2H^+ is less affected by depletion. Therefore, N_2H^+ appears in gas-phase when CO is already depleted and H_2D^+ is already abundant.

D-fractionation towards massive star-forming regions

Can the results described above be applied to the high-mass regime? As already said, the theory of massive star-formation is still not well-understood and, moreover, the observations are challenging since these regions are at large distances (>1 kpc), and hence they have small angular sizes. Moreover, clustered environments make observations of the process challenging. However, in the last decade many studies have been performed to check if the chemical properties observed in the earliest stages of low-mass stars are also valid for high-mass star-forming regions. In this section I will go through the main papers that studied, until now, the problem of deuterium fractionation towards these regions.

Fontani et al. (2006) observed N_2H^+ and N_2D^+ towards 10 high-mass protostellar candidates, selected from the samples described by Molinari et al. (1996) and Sridharan et al. (2002). These molecules were chosen since they can form only in gas-phase, and then they are appropriate to trace deuteration occurring through gas-phase chemistry. They found $D_{\rm frac}(N_2H^+)$ between ∼0.004 and ∼0.02, with an average value of 0.015, 3 orders of magnitude higher than the PSN value, and quite close to the values found by Crapsi et al. (2005) in a sample of low-mass starless cores.

Fontani et al. (2011) expanded the previous work observing with the IRAM 30m telescope N_2H^+ and N_2D^+ towards 27 high-mass star-forming cores divided into different evolutionary stages of the massive star-formation process, already described in Sect. 1.2: high-mass starless cores (HMSCs), high-mass protostellar objects (HMPOs) and UC HII regions. They found a high N_2D^+ detection rate (>65%) towards each evolutionary stage, meaning that deuterated gas is present at every stage of massive star formation. The main result is that HMSCs have an average $D_{\rm frac}(N_2H^+)$ of ∼0.26, while HMPOs and UC HIIs have an average $D_{\rm frac}(N_2H^+)$ of ∼0.037 and ∼0.044, respectively: the difference between HMSCs and both HMPOs and UC HIIs is statistically significant, and shows that $D_{\rm frac}(N_2H^+)$ decreases by an order of magnitude from the starless to the protostellar phases in both low- and high-mass star-forming cores.

Sakai et al. (2012) measured for the first time the D-fractionation for HNC in a sample of 18 massive cores including IRDCs and HMPOs. They found that $D_{\rm frac}$(HNC) in the starless cores is only marginally higher than that measured in the protostellar cores. This could be explained by the faster destruction processes of N_2D^+ than those of DNC. In fact, N_2D^+ can recombine quickly with CO or electrons, while DNC has to be destroyed by ions, like HCO^+, through much slower (10^4–10^5 yr) chemical reactions. In particular, chemical

calculations show that the N_2D^+/N_2H^+ ratio is ∼0.1 during the cold pre-stellar phase and drops quickly to ∼0.01 after the protostellar birth since it is very sensitive to the temperature growth (Fontani et al. 2014, right panel of Fig. 1.11).

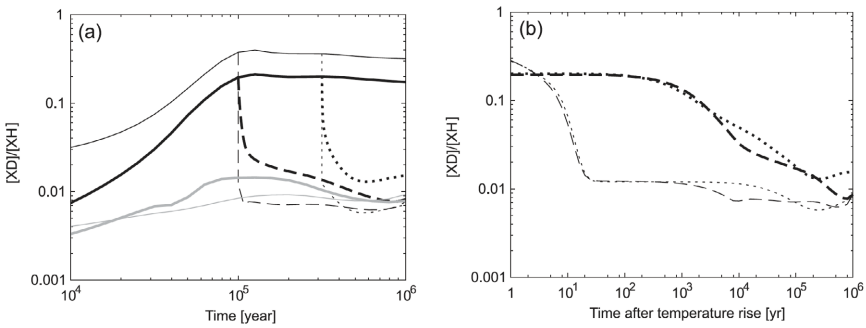

Fig. 1.11: Chemical model calculation of the time dependence of DNC/HNC (thick lines) and N_2D^+/N_2H^+ (thin lines) made by Fontani et al. (2014). *Panel (a):* the constant temperature cases are the solid black (10 K) and the solid grey (30 K) lines. The other lines represent the cases in which the temperature rises from 10 to 30 K at an age of 1×10^5 yr (dashed) or 3×10^5 yr (dotted). *Panel (b):* same as left panel but the time starts when the temperature increases from 10 to 30 K.

To allow for a consistent observational comparison between the deuterated fraction of N_2H^+ and HNC, Fontani et al. (2014) observed the D-fractionation of HNC towards a sub-sample of the sources used in Fontani et al. (2011). They found for the HMSCs an average $D_{\rm frac}$(HNC)∼0.012, and for the HMPOs and UC HII very similar average values of ∼0.009 and ∼0.008, respectively. This supports the results by Sakai et al. (2012), that $D_{\rm frac}$(HNC) does not change significantly going from the colder phase to the active star formation phases. Thus, there is a clear different behaviour between $D_{\rm frac}$(HNC) and $D_{\rm frac}(N_2H^+)$ in high-mass star-forming cores. In particular, the first is less sensitive to a temperature rise and the second is more suitable to identify HMSCs: $D_{\rm frac}(N_2H^+)$ of ∼0.2–0.3 should signpost good candidate massive pre-stellar cores. A similar result has been found more recently by Imai et al. (2018) towards a sample of young protostars with a strong accretion and more evolved objects that have already accreted their final mass, still embedded in their cold envelope.

However, N_2H^+, HNC and their deuterated isotopologues can form mainly (HNC, DNC) or solely (N_2H^+, N_2D^+) in the gas phase. Other important molecules, like NH_3, CH_3OH and their deuterated forms, can be produced on dust grain surfaces, and theoretical models show that their $D_{\rm frac}$ could be different than that of gas-phase species, especially during the protostellar phase in which grain mantles evaporate. Fontani et al. (2015a) investigated the role of surface chemistry through observations of ammonia, methanol

and their deuterated species (NH_2D, CH_2DOH, CH_3OD).The main conclusion of this work is that N_2D^+/N_2H^+ is the only ratio which shows a statistically significant decrease from HMSCs to HMPOs. Recently, Ospina-Zamudio et al. (2019) investigated the deuteration of methanol towards the high-mass star-forming region NGC7538-IRS1. Their study showed that the fractionation degree of deuterated methanol is low in this source $\sim$1–3$\times10^{-4}$, and a CH_2DOH/CH_3OD relative abundance of 3.2$\pm$1.5. These results are consistent with the hypothesis that deuterium fractionation of methanol proceeds in the ice during the early cold pre-stellar phase through the statistical addition of H and D atoms to CO molecules (e.g. Faure et al. 2015; Bøgelund et al. 2018).

Even though the CO depletion is expected, in theory, to be lower in high-mass star-forming regions, because they are warmer since the early phases, observations show that CO depletion is also efficient for these objects. To estimate the CO depletion, a factor called CO depletion factor (f_D) is commonly used. It is defined as the ratio between the expected abundance of CO relative to H_2 (derived taking into account the atomic carbon and oxygen abundances with distance to the Galactic center) and the observed value. For example, Fontani et al. (2012) and Sabatini et al. (2019) found f_D of $\sim$10 or more, i.e. even larger that in low-mass pre-stellar cores, towards the innermost regions of IRDCs. Moreover, Giannetti et al. (2014), using observations of the ATLAS survey towards massive clumps, found that CO depletion in these clumps seems to behave as in the low-mass regime, with less evolved clumps showing larger values for the depletion than their more evolved counterparts, and increasing for denser sources.

1.4.4. Nitrogen fractionation in the ISM

First chemical models

The possibility of nitrogen isotopic fractionation in interstellar clouds was discussed for the first time by Terzieva and Herbst (2000). In cold dense environments the only source of fractionation was expected to be isotope-exchange reactions, as already explained for deuterium fractionation. Adams and Smith (1981) studied in laboratory the system

$$N_2H^+ + {}^{15}NN \rightleftharpoons {}^{15}NNH^+ + N_2. \tag{1.31}$$

They found that the forward reaction is the exothermic direction, but that the exothermicity is small and expected to lead a small amount of fractionation in clouds with a temperature lower than 10 K. Thus, Terzieva and Herbst (2000) decided to theoretically study a variety of possible ion-molecule isotopic exchange reactions involving abundant N-containing species. Their study was based on a statistical mechanical approach to derive the rate coefficients (see Sect. 1.3). They considered fractionation from molecular, neutral and ionised

atomic nitrogen, and derived the exothermicity for all of the cases. They set the forward reaction rate coefficient to be equal to a fraction of the Langevin collisional rate ($k_{\rm L}$= $8.1{\times}10^{-10}{\rm cm}^{-3}{\rm s}^{-1}$). They modelled a system with a number density $n_{\rm H}$ of $2{\times}10^4$ cm^{-3}, a cosmic-ray ionisation rate ζ for H_2 of $1.3{\times}10^{-17}$ s^{-1}, and temperatures from 10 K up to 40 K. The main finding of this work was that exchange reactions between ^{15}N atoms and N-containing ions are the main contributors to N-fractionation. However, they did not find a large amount of fractionation between different molecules.

Charnley and Rodgers (2002) showed that, as for D-fractionation, gas-grain effects could lead to significant ^{15}N-fractionation. In fact, under normal interstellar conditions, N_2 is the dominant form of nitrogen, and ^{14}N and ^{15}N are continuously cycled in gas-phase through the sequence

$$N_2 \xrightarrow{He^+} N \xrightarrow{OH} NO \xrightarrow{N} N_2, \tag{1.32}$$

that cycles nitrogen between atomic and molecular form (see also Fig. 1.12).

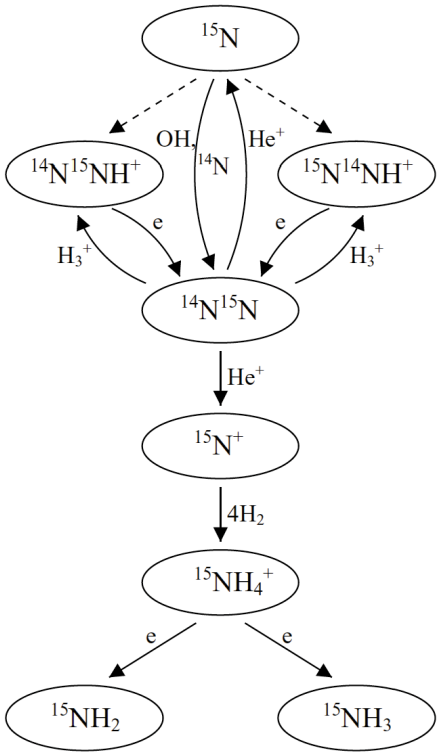

Fig. 1.12: Main gas-phase reactions involving nitrogen included in Charnley and Rodgers (2002) and Rodgers and Charnley (2008a) chemical networks.

The first step of this cycle produces also N^+, which reacts with molecular hydrogen and leads to ammonia. When O/C-bearing molecules freeze out on ice mantles, there is insufficient OH to drive the above cycle. This leads to more nitrogen atoms in each of the isotopic forms. Charnley and Rodgers (2002) considered the effect in the context of dense pre-stellar cores adopting a gas density of 10^7 cm^{-3} and a temperature of 10 K. They found that most of the atomic ^{15}N goes in N_2H^+ through the reactions

$$N_2H^+ + {}^{15}\mathrm{N} \rightleftharpoons {}^{15}\mathrm{NNH}^+ + \mathrm{N}, \tag{1.33}$$

and

$$N_2H^+ + {}^{15}\mathrm{N} \rightleftharpoons \mathrm{N}{}^{15}\mathrm{NH}^+ + \mathrm{N}. \tag{1.34}$$

Moreover, when the electronic dissociative recombination of $^{15}NNH^+$ and $N^{15}NH^+$ is efficient, this excess of N-fractionation reflects into an enhanced abundance of $^{15}N^{14}N$, which, subsequently, could cause an excess of $^{15}N^+$ through the first step of the cycle shown in (1.32). The excess of $^{15}N^+$ leads to fractionation of $^{15}NH_3$, which then depletes onto ices. The main nitrogen isotopic-exchange reactions used in their chemical network are schematised in Fig. 1.13.

Rodgers and Charnley (2008a) revised their chemical model to take into account new experimental results for the branching ratio of the dissociative recombination of N_2H^+:

$$N_2H^+ + e^- \rightleftharpoons N_2 + H \quad (1-f), \tag{1.35}$$

$$N_2H^+ + e^- \rightleftharpoons NH + N \quad (f). \tag{1.36}$$

They considered values for f=0, 0.02 and 0.05 (Molek et al. 2007). Moreover, they also tracked the $^{14}N/^{15}N$ in different monolayers of ammonia ice on grain surfaces. With these updates they could recover the results of the earlier work in dense, CO-depleted gas at 10 K, finding that the uppermost layers, which accrete later, have the largest ^{15}N-enrichments.

However, these models can not reproduce the CN abundances derived towards the pre-stellar cores L1544 and L183 ($\sim 2\times10^{-9}$, Hily-Blant et al. 2008). Rodgers and Charnley (2008b) reassessed the ^{15}N chemistry to shed light to these new observational evidences. They found that enhanced ^{15}N in nitrile-bearing species is possible, at an early time, via the reactions

$$\mathrm{HC}{}^{14}\mathrm{NH}^+ + {}^{15}\mathrm{N} \rightleftharpoons \mathrm{HC}{}^{15}\mathrm{NH}^+ + {}^{14}\mathrm{N}. \tag{1.37}$$

All of the discussion until now takes into account only the role of isotopic-exchange reactions between ion and neutral molecules. Thus, Rodgers and Charnley (2008b) studied for the first time the possible role of neutral-neutral reactions involving ^{15}N and CN. In particular, they extimated that the reaction

$$\mathrm{C}{}^{14}\mathrm{N} + {}^{15}\mathrm{N} \rightleftharpoons \mathrm{C}{}^{15}\mathrm{N} + {}^{14}\mathrm{N} \tag{1.38}$$

has an exothermicity of 35 K and found that this could be important for ^{15}N-fractionation of nitrile-bearing species at early times.

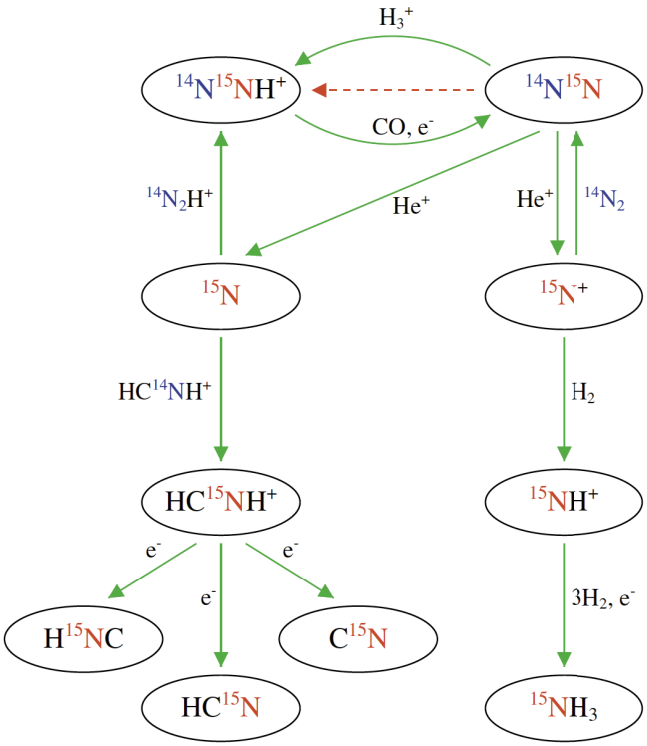

Fig. 1.13: Chemical network showing the main isotopic-exchange reactions responsibile for ^{15}N-enhancements in molecules. Taken from Wirström et al. (2012).

Recent observations and related chemical models

PRE-STELLAR CORES: Even if some models for pre-stellar cores were already available before 2000, observations started to constrain them only later, during the last decade.

Gerin et al. (2006) already demonstrated that multiply deuterated ammonia can be very abundant in low-mass pre-stellar cores, and Gerin et al. (2009) derived a $NH_2D/^{15}NH_2D$ abundance ratio from 360 to 810 in a small sample of pre-stellar cores. These ratios are comparable with that of the PSN (441). Subsequently, Lis et al. (2010) derived the $^{14}N/^{15}N$ in ammonia towards two cold, dense molecular clouds, Barnard 1 and NGC 1333. They found a $^{14}N/^{15}N$ of 334±50 and 344±173, respectively. These values are in between the TA value (270) and the PSN one, and can be reproduced only by a gas-phase model that approximates the adsorption on grain surfaces by reducing the elemental abundances in the gas (Gerin et al. 2009), and not by Rodgers and Charnley (2008b) that take into account the mantle formation and gas-grain interactions. This suggested that many observations, also of other molecules, were

needed to constrain chemical models at that time.

Following the results of Rodgers and Charnley (2008b), Bizzocchi et al. (2010) detected for the first time the ^{15}N-containing diazenylium ion (N_2H^+) in the pre-stellar core L1544. To prove if the nitrogen fractionation process is at work in the way described by the models (e.g. Rodgers and Charnley 2008b), L1544 was a perfect target since it was found to have N_2D^+/N_2H^+ ratio of 0.25, and since its central region could reach a temperature of 5.5 K (Crapsi et al. 2007), which is expected to enhance the ^{15}N in molecules. They found a $N_2H^+/N^{15}NH^+$ abundance ratio of 446±71, very similar to the PSN value, and different from what predicted by chemical models. However, Bizzocchi et al. (2013) revised these results by performing a non-LTE analysis, using the physical model proposed for this source by Keto and Caselli (2010). From this new analysis they found $^{14}N/^{15}N$= 1000±200, even more difficult to explain with cold gas-phase isotopic-exchange reaction models.

Wirström et al. (2012) proposed a new chemical network, taking into account both D- and ^{15}N-enrichments in molecules, with the novelty of including the spin-state of H_2, H_2^+ and H_3^+. The major interstellar collision partner, molecular hydrogen, has a 170.5 K difference in zero-point energy between the *para* (*p*, anti-parallel spins) and the *ortho* (*o*, parallel spins) form, with the *o*-H_2 being the higher energy one. Thus, the *ortho*-to-*para* ratio (OPR) can influence the energy balance in exothermic reactions in which H_2 is involved, and hence could affect N-fractionation as well. For example, the reaction

$$N^+ + H_2 \rightarrow NH^+ + H, \tag{1.39}$$

followed by three other reactions with H_2, is important for ammonia formation (see Fig. 1.12), but it presents an activation energy of 200 K that at low temperature could be overcome only by the internal energy of *o*-H_2 (Le Bourlot 1991). Moreover, Dislaire et al. (2012) evaluated from experimental data a different rate coefficient for reaction (1.39) depending on the spin of H_2. So, ammonia fractionation becomes much less efficient as the OPR decreases, and then, as illustrated in Fig. 1.13, an increasing quantity of $^{15}N^+$ goes back into molecular nitrogen by

$$^{15}N^+ + ^{14}N_2 \rightleftharpoons ^{14}N^+ + ^{15}N^{14}N. \tag{1.40}$$

Thus, while the time evolution of the system shows an *o*-H_2 drop, a substantial rise in the ammonia $^{14}N/^{15}N$ is also present, up to almost doubling the PSN value ($\lesssim$800, see Fig. 1.14). This suggests an age for the fractionated ammonia in L1544 (Gerin et al. 2009) of $\sim 3\times10^5$ yr. Moreover, Wirström et al. (2012) found that while HCN and HNC are enriched in ^{15}N for shorter time scales ($t\sim 2\times10^5$), this is not true for deuterium. However, the results obtained by Bizzocchi et al. (2013) remain puzzling even with this new model since it is expected that N_2H^+ derives from the molecular nitrogen via the protonation reaction

$$N_2 + H_3^+ \rightarrow N_2H^+ + H_2, \tag{1.41}$$

and then it is expected that the $^{14}N/^{15}N$ of N_2H^+ follows that of N_2, i.e. that it diminishes (see Fig. 1.14).

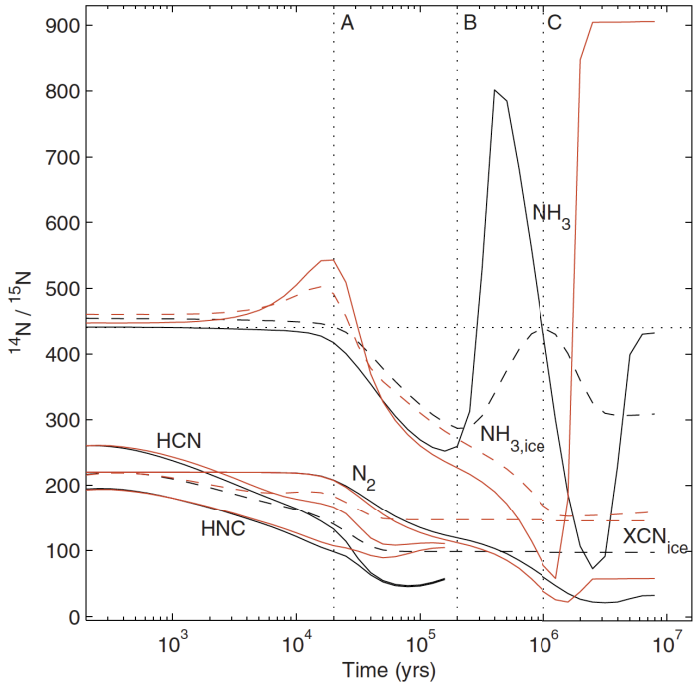

Fig. 1.14: Time evolution of the $^{14}N/^{15}N$ in molecules in gas-phase, and some species in the ice. The black curves represent the results by Wirström et al. (2012), and the red ones the results by Rodgers and Charnley (2008a). The dotted horizontal line represents the PSN value of 441. Taken from Wirström et al. (2012).

In Fig. 1.15 the main reaction routes for nitrogen molecules in a cold (10 K) cloud are summarised. It can be noted that N-bearing molecules can be divided into two families: nitriles (-CN) and amines (-NH). The former form directly from atomic nitrogen, while the latter form from N^+ that is a product of molecular nitrogen. In this sense it is not expected that these two families could exchange ^{15}N, and therefore different $^{14}N/^{15}N$ are predicted. In fact, Hily-Blant et al. (2013a) observed $^{14}N/^{15}N$ of nitrile-bearing species towards pre-stellar cores, to compare models and observations for these molecules. They performed a non-LTE analysis of the fundamental rotational transition of $H^{13}CN$ and $HC^{15}N$ towards the two starless cores L1544 and L183. Adopting a $^{12}C/^{13}C$ of 68 (Milam et al. 2005) they obtained $HCN/HC^{15}N$ ratios from 140 to 360 towards L1544, and from 140 to 250 towards L183. In both sources the high values were measured near the center of the core. These values are significantly lower than that derived from ammonia and N_2H^+, suggesting a

differential behaviour in the N-fractionation of nitriles and amines, as already predicted by Rodgers and Charnley (2008b).

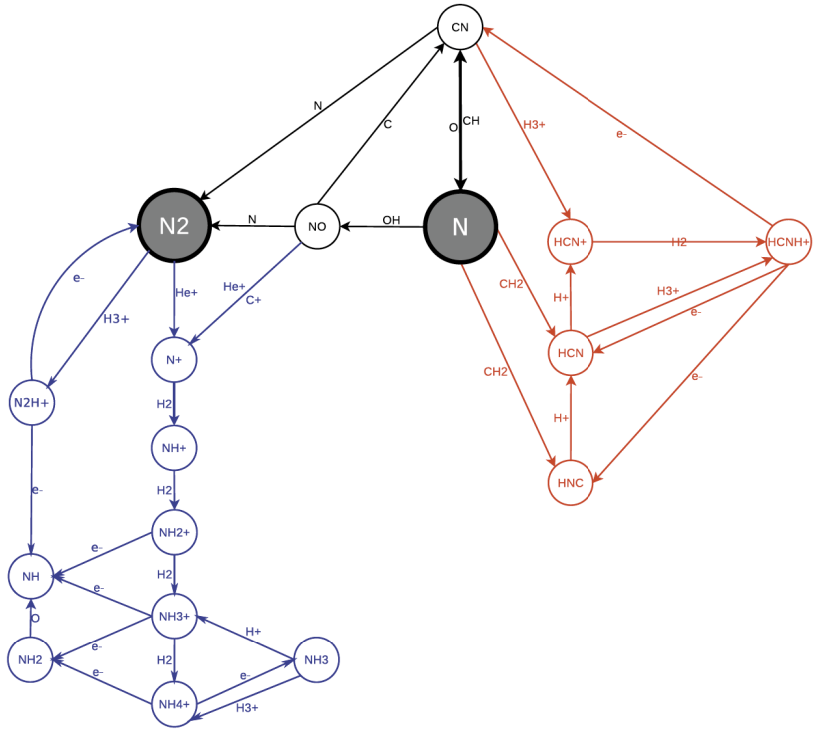

Fig. 1.15: Main chemical routes involving nitrogen-bearing molecules. The routes are clearly separate in two groups, the one containing amine group (blue), and those containing nitrile-bearing species (red). Taken from Hily-Blant et al. (2013a).

From Fig. 1.15 it is clear that evaluating the ^{15}N-fractionation of CN towards pre-stellar cores could be useful to understand the chemical processes that are mainly responsible for the observed isotopic ratios because it is a mediator of the atomic-to-molecular nitrogen conversion. In this context, Hily-Blant et al. (2013b) obtained towards L1544 and L1498 obtaing an average ^{14}N/^{15}N of 500±75 from CN. This ratio is larger than those obtained from HCN and is similar to some values observed from hydrides towards dark clouds (e.g. Gerin et al. 2009; Lis et al. 2010). These new results gave new constraints to chemical models. Hily-Blant et al. (2013b) implemented N-fractionation reaction in a gas-phase dark cloud chemical model ($n_{\rm H}$=10^4 cm^{-3} and T=10 K), modifying the rate of reactions to the more updated one, as the *ortho–para* conversion of H_2 through proton exchange reactions (Rist et al. 2013). Their model predicted that HCN, HNC and NH were positively fractionated, while N, NO, and CN were not.

Until 2013, most of the observational studies focused on a single species. Daniel et al. (2013) studied for the first time N-fractionation in the same object in several species, such as N_2H^+, NH_3, CN, HCN and HNC, towards the low-mass pre-stellar core B1b. The main result of this work is that they did not find any substantial differential fractionation between the nitrogen hydride and nitrile-bearing species, with an average value of ∼296. A possible explanation of this is the gas temperature in the core center of B1b, estimated to be 17 K, and then higher than the temperature reached during the low-mass pre-stellar phase. Regarding N_2H^+, they found a value lower than that obtained towards L1544 by Bizzocchi et al. (2013). Subsequently, Daniel et al. (2016) targeted the pre-stellar core 16293E and derived a $N_2H^+/N^{15}NH^+$=330±150, which is still lower than that of L1544, and again a possible explanation could be a difference in the central temperature of the core. However, chemical models are not able to reproduce this dependence of fractionation with the temperature.

PROTOSTELLAR OBJECTS: To better understand the link between the pristine Solar system materials and the PSN, evolutionary stages more evolved than pre-stellar cores should be investigated. Wampfler et al. (2014) studied the $^{14}N/^{15}N$ ratio around three nearby low- to intermediate-mass protostars, to investigate whether the signature of nitrogen isotope fractionation also occurs in the embedded protostellar stages, and if they show differences from both the early pre-stellar phase and the Solar system objects. In fact, apart from low-temperature isotopic-exchange reactions, Liang et al. (2007) demonstrated that also isotopic-selective photodissociation of N_2 could play an important role in the explanation of ^{15}N anomalies in the upper atmosphere of Titan. Wampfler et al. (2014) derived $^{14}N/^{15}N$ ratio for HCN and HNC and they found values for two sources similar to those measured in pre-stellar cores (160–280). However, for the third source, OMC-3 MMS6, they found higher values similar to the PSN one. They proposed as explanation for this difference, the amount of external irradiation the sources are exposed to. In fact, OMC-3 MMS6 is exposed to an enhanced radiation field, resulting in a warmer outer envelope with respect to the other sources. This would argue in favour of chemical fractionation scenario, and against isotope-selective photochemistry. However, to what extent this latter mechanism could have affected the nitrogen isotope composition of the PSN is not clear yet.

PROTOPLANETARY DISCS: Another important evolutionary stage is that of protoplanetary discs since they are the cradle in which protoplanets form. Thus, distinguishing between the different origins of nitrogen isotopic ratios in discs is a key point. In particular, the radial and vertical trends of the $^{14}N/^{15}N$ ratio in each disc would indicate the processes that influence and regulate this fraction. In theory, a constant $^{14}N/^{15}N$ ratio across each disc would favour a scenario where discs inherit their molecular complexity from the natal cloud, while a radial gradient would point to disc chemistry induced by irradiation from the nascent star.

Guzmán et al. (2015) presented the first measurement of the HCN/HC^{15}N in a disc, in particular the protoplanetary disc around the Herbig Ae star MWC 480. They found from Atacama Large Millimeter Array (ALMA) observations an average ^{14}N/^{15}N of 200±100, which is consistent with what is observed in comets. Later, Guzmán et al. (2017) presented 0.5″ angular resolution observations of the J=3–2 transition of H^{13}CN and HC^{15}N towards a sample of six protoplanetary discs. To derive the nitrogen fractionation in HCN, they adopted an isotopic ^{12}C/^{13}C ratio of 70. The measured nitrogen isotope ratios range from 83±37 up to 156±78, which is consistent with a constant disc-averaged fractionation level, within the errors. This sample of discs consisted of 4 T Tauri discs and 2 Herbig Ae discs, and they found no differences in the ^{15}N-enhancement level between the two groups of discs that have an order of magnitude difference in the stellar radiation field. Finally, towards the disc V4046 Sgr they found an indication of increasing ^{14}N/^{15}N ratio from the inner to the outer part of the disc. This points to an active nitrogen fractionation, suggesting that selective photodissociation induced by the protostellar radiation field is important to fractionate HCN in the inner disc. However, high-angular resolution observations are needed towards more discs to determine if this is a general trend for protoplanetary discs or if V4046 Sgr is a special case. Another evidence that isotopic-exchange reactions do not contribute alone to N-fractionation in discs is the fact that Guzmán et al. (2017) did not find a correlation between D/H (measured by Huang et al. 2017) and ^{14}N/^{15}N ratio in the sample. Finally, Hily-Blant et al. (2017) directly measured a CN/C^{15}N ratio of 323±30 in the disc orbiting TW Hya. The comparison with the HCN/HC^{15}N ratios measured towards other discs, demonstrates that CN and HCN in discs are not tracing the same reservoirs, as already shown in pre-stellar cores (Hily-Blant et al. 2013b).

Visser et al. (2018) present the first 2D disc model that includes both low-temperature isotope-exchange reactions and isotope-selective photodissociation of N_2, finding that for nitrile-bearing species nitrogen isotope fractionation is fully dominated by the second process, and that low-temperature exchange reactions do not contribute at all.

Fig. 1.16 summarises all of the literature values described in this chapter. This figure will be updated in next chapters with more recent results, including those of this thesis.

Updated chemical networks: new predictions from chemical models

Roueff et al. (2015): They studied the fractionation processes in the ISM, re-investigating the study of Terzieva and Herbst (2000). They used a time-dependent gas-phase chemical model, including also the effects of ^{12}C/^{13}C on nitrogen fractionation of nitrile-bearing species. If experimental information was available they constrained the rate constants of reactions using it. Conversely, if no experimental data were available, they checked for the possible

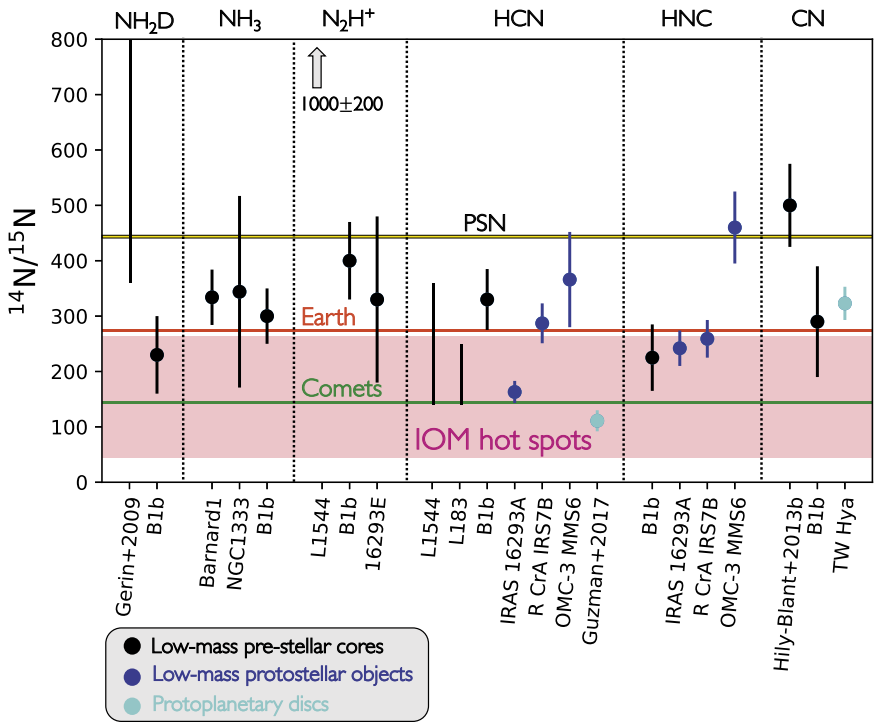

Fig. 1.16: $^{14}N/^{15}N$ ratios obtained for different molecules, as described in Sect. 1.4.4. Black points represent low-mass pre-stellar cores, the blue points are low-mass protostellar objects, and the cyan points indicate protoplanetary discs. The horizontal yellow and red solid lines represent the PSN value of 441 and the TA value of 272, respectively. The green horizontal line denotes the average value measured in comets. Moreover, the pink area represents measurements in carbonaceous chondrites, where the lower ones are the so-called "hot-spots".

presence of barriers in the entrance channels of isotopic-exchange reactions through theoretical calculations, and updated the ZPE values involved, deriving the corresponding exothermicity values. In Table 1.1 all the isotopic-exchange reactions taken into account in this work, for N and C, are listed. In particular, for reaction (11) they were able to evaluate an upper limit for the rate coefficient, but they did not take it into account in their model. The type of reactions, given in the first column of the table, are summarised as follows:

- A - *direct reactions*: the equilibrium coefficient K is defined as in eq. 1.15;
- B - *reactions involving adduct formation, without isomerization*: the statistical theory for the system at thermal equilibrium is applied. Thus, k_f

$+ k_r = k_{capture}$. From the equilibrium coefficient K, it can be derived that $k_f = k_{capture} \times \frac{f(B,M)}{[f(B,M)+\exp(-\Delta E/k_B T)]}$;

- C - *reactions involving adduct formation, with isomerization*: isomerization reaction rate estimated with statistical calculation, and the rate constant depends on the location of the transition state. It is required to study in detail case by case;

- D - *other type of reactions*: generally these reactions are discarded.

Moreover, they have also included chemical reactions involving nitrogen atoms and CH, CN, and OH that have been studied experimentally. Thus, they have updated their chemical network with the corresponding reaction rate constants that have been implemented in the KIDA chemical database (Wakelam et al. 2013).

They considered two different models, where the model (a) is a template of TMC-1, with a density n_H of 2×10^4 cm^{-3}. Model (b) is more representative of a pre-stellar core with a density n_H of 2×10^5 cm^{-3}, similar to L134N or Barnard 1. Both models presented a cosmic ray-ionisation rate ζ for H_2 of 1.3×10^{-17} s^{-1} and a temperature of 10 K.

As in Wirström et al. (2012) they also took into account the possible role of the *ortho/para* molecular hydrogen into N-fractionation, in particular for the ^{15}N-enhancement of ammonia. They considered the different rate coefficient for reaction (1.39) depending on the spin of H_2, as discussed by Dislaire et al. (2012). They also extended the analysis of reaction (1.39) to deuterated forms and those including ^{15}N. In the case of ^{15}N substituted compounds they took into account the small additional term due to the change in ZPE. They found that, since the $N^+ + HD \rightarrow ND^+ + H$ reaction is less exothermic than $N^+ + H_2 \rightarrow NH^+ + H$ reaction, this creates a $NH_3/^{15}NH_3$ ratio that is higher than $NH_2D/^{15}NH_2D$ at steady state (see Fig. 1.17).

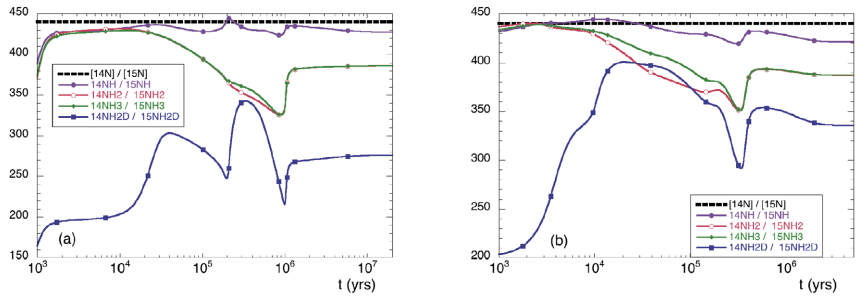

Fig. 1.17: Time dependence of $^{14}N/^{15}N$ isotopic ratios of NH, NH_2, NH_3 and NH_2D found by Roueff et al. (2015). The panels a) and b) correspond to the models defined in the text; the black dotted line represents the elemental $^{14}N/^{15}N$. Taken from Roueff et al. (2015)

Table 1.1: ^{15}N and ^{13}C isotopic-exchange reactions used by Roueff et al. (2015).

Label/ comment	Reaction	k_f ($cm^3\ s^{-1}$)	$f(B,m)$	ΔE (K)
(1) A	$N^{15}N + N_2H^+ \rightleftharpoons N^{15}NH^+ + N_2$	2.3×10^{-10}	0.5	10.3
(2) A	$N^{15}N + N_2H^+ \rightleftharpoons {}^{15}NNH^+ + N_2$	2.3×10^{-10}	0.5	2.1
(3) A	$N^{15}N + {}^{15}NNH^+ \rightleftharpoons N^{15}NH^+ + N^{15}N$	4.6×10^{-10}	1	8.1
(4) B	$^{15}N^+ + N_2 \rightleftharpoons {}^{14}N^+ + N^{15}N$	$4.8\times10^{-10} \times \frac{2}{2+\exp(-28.3/T)}$	2	28.3
(5) C	$^{15}N + CNC^+ \rightleftharpoons C^{15}NC^+ + {}^{14}N$	$3.8\times10^{-12} \times (\frac{T}{200})^{-1}$	1	38.1
(6) barrier	$^{15}N^+ + {}^{14}NO \rightleftharpoons {}^{14}N^+ + {}^{15}NO$	no react	–	24.3
(7) barrier	$^{15}N + N_2H^+ \rightleftharpoons {}^{14}N + N^{15}NH^+$	no react	–	38.5
(8) barrier	$^{15}N + N_2H^+ \rightleftharpoons {}^{14}N + {}^{15}NNH^+$	no react	–	30.4
(9) barrier	$^{15}NNH^+ + H \rightleftharpoons H + N^{15}NH^+$	no react	–	8.1
(10) barrier	$^{15}N + HCNH^+ \rightleftharpoons {}^{14}N + HC^{15}NH^+$	no react	–	37.1
(11) D	$^{15}N + CN \rightleftharpoons {}^{14}N + C^{15}N$	$<2.0\times10^{-10}\times (\frac{T}{300})^{1/6}\times \frac{1}{1+\exp(-22.9/T)}$	1	22.9
(12) B	$^{15}N + C_2N \rightleftharpoons {}^{14}N + C_2{}^{15}N$	$1.6\times10^{-10} \times (\frac{T}{300})^{1/6} \times \frac{1}{1+\exp(-26.7/T)}$	1	26.7
(13) D	$^{15}N + {}^{14}NO \rightleftharpoons {}^{14}N + {}^{15}NO$	– (neglected)	–	24.3
(14) B	$^{13}C^+ + CO \rightleftharpoons {}^{12}C^+ + {}^{13}CO$	$6.6\times10^{-10}\times (\frac{T}{300})^{-0.45}\times \exp(-6.5/T)\times \frac{1}{1+\exp(-34.7/T)}$	1	34.7
(15) A	$^{13}CO + HCO^+ \rightleftharpoons CO + H^{13}CO^+$	$2.6\times10^{-12}\times (\frac{T}{300})^{-0.4}$	1	17.4
(16) B	$^{13}C^+ + CN \rightleftharpoons {}^{12}C^+ + {}^{13}CN$	$3.82\times10^{-9}\times (\frac{T}{300})^{-0.4}\times \frac{1}{1+\exp(-31.1/T)}$	1	31.1
(17) B	$^{13}C + CN \rightleftharpoons {}^{12}C + {}^{13}CN$	$3.0\times10^{-10}\times \frac{1}{1+\exp(-31.1/T)}$	1	31.1
(18) C	$^{13}C + HCN \rightleftharpoons {}^{12}C + H^{13}CN$	– (neglected)	–	48.4
(19) B	$^{13}C + C_2 \rightleftharpoons {}^{12}C + {}^{13}CC$	$3.0\times10^{-10}\times \frac{2}{2+\exp(-26.4/T)}$	2	26.4
(20) barrier	$^{13}CH + CO \rightleftharpoons {}^{13}CO + CH$	no react	–	28.6

One of the important results that they obtained is that the fractionation reaction of ^{15}N with N_2H^+ is unlikely due to the presence of a barrier. This is in contrast with the previous chemical models by Terzieva and Herbst (2000) and Rodgers and Charnley (2008a). The main consequence is that the modeled N-isotopic ratio for N_2H^+ is found to be very close to the PSN value of 441. However, this value is still in contradiction with observations towards L1544 (Bizzocchi et al. 2013). Moreover, the different endothermicity in the reactions of $^{15}NNH^+$ and $N^{15}NH^+$ with N_2 leads to the prediction that $^{15}NNH^+$ should

be less abundant than $N^{15}NH^+$ (see Fig. 1.18).

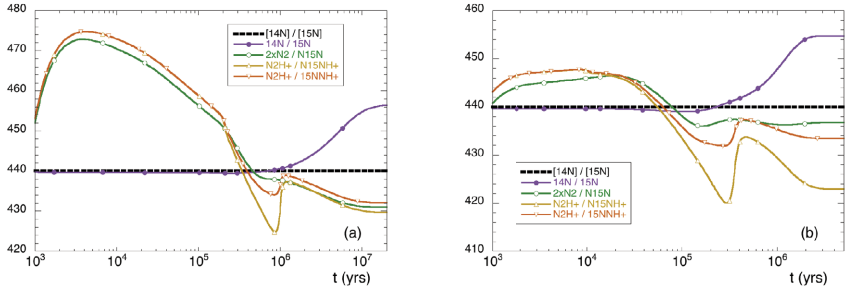

Fig. 1.18: Time dependence of $^{14}N/^{15}N$ isotopic ratios of atomic and molecular nitrogen and N_2H^+ ions found by Roueff et al. (2015). The panels a) and b) correspond to the models defined in the text; the black dotted line represents the elemental $^{14}N/^{15}N$. Taken from Roueff et al. (2015)

With the same argument of the presence of a barrier, they also discarded the ^{15}N + $HCNH^+$ and ^{15}N + NO exchange reactions. In particular, discarding the first one results in a predicted $^{14}N/^{15}N$ for nitrile-bearing species not different from the elemental value (Fig. 1.19). Moreover, since they also included a treatment for C-fractionation, they were able to compare their results directly with observations of N-fractionation in nitrile-bearing species. In fact, one of the methods to evaluate $^{14}N/^{15}N$ ratios for nitriles is with the double-isotopes method, that includes observations of the species containing the ^{13}C-isotopologue to avoid optical depth problems. Then, an elemental $^{12}C/^{13}C$ ratio have to be assumed to evaluate the $^{14}N/^{15}N$ ratio. They found that the deviation from the elemental value $^{15}N/^{13}C$=6.5[10] is significant for HNC, HCN, and CN: 4 for HNC and HCN and almost 7 for CN (Fig. 1.20). The $^{12}C/^{13}C$ ratio time dependence will be discussed in detail in chapter 5.

Wirström and Charnley (2018): Wirström and Charnley (2018) re-evaluated the calculation by Wirström et al. (2012) in light of the revised Roueff et al. (2015) fractionation chemistry, since there are significant physical and chemical differences in these two models. In particular, Wirström et al. (2012) considered densities similar to pre-stellar core conditions (n_{H_2} of 10^6 cm^{-3}, a temperature of 10 K, a cosmic-ray ionisation rate ζ for H_2 of 3×10^{-17} s^{-1}). Moreover, Roueff et al. (2015) did not include the depletion of gas-phase species by freeze-out on dust grains, nor the time dependence in the H_2 OPR. In their work Wirström and Charnley (2018) investigated the possible role of the reaction (11) of Table 1.1, since it was demonstrated that the reaction

$$N + CN \rightarrow N_2 + C \tag{1.42}$$

[10] $(^{15}N/^{14}N)\times(^{12}C/^{13}C)$=400/68=6.5.

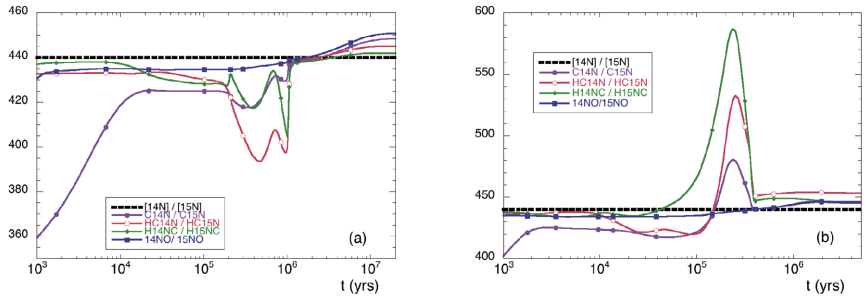

Fig. 1.19: Time dependence of $^{14}N/^{15}N$ isotopic ratios of CN, HNC, HCN and NO found by Roueff et al. (2015). The panels a) and b) correspond to the models defined in the text; the black dotted line represents the elemental $^{14}N/^{15}N$. Taken from Roueff et al. (2015)

does not present a barrier, and Roueff et al. (2015) found that the isotopic exchange reaction between ^{15}N and CN is plausible. Wirström and Charnley (2018) updated also the model with respect to the specific reaction in the nitrogen chemistry from KIDA database, as already done by Roueff et al. (2015). As initial condition they assumed an elemental $^{14}N/^{15}N$ ratio of 440 with the same initial abundance of ^{15}N and $^{14}N^{15}N$ ($^{15}N/^{14}N^{15}N$=1). This implies a nominal $N_2/^{14}N^{15}N$ ratio of 220.

They followed two different approaches:

- First of all, they compared the results obtained by Wirström et al. (2012) with those obtained updating the old network with only the new reaction rates of isotopic-exchange reactions in Table 1.1. The most important fractionation reactions are shown in Fig. 1.21, and following this network they found an enhancement of a factor ∼10 in nitrile-bearing species with respect to the results given by Roueff et al. (2015) (see Fig. 1.22). This behaviour is due to the atomic ^{15}N that rapidly fractionates CN through the reactions (5) and (11) of Table 1.1. Moreover, this ^{15}N-enhancement is successively spread to HCN, e.g. through the reaction

$$CN + NH_3 \rightarrow HCN + NH_2, \tag{1.43}$$

  and later to HNC through dissociative electron recombination of $HCNH^+$, formed by reactions of HCN with HCO^+ and H_3O^+.

  They also found that NH_3 is not enhanced in ^{15}N because reaction (4) of Table 1.1 allows a faster creation of $N^{15}N$ starting from $^{15}N^+$, than the creation of $^{15}NH^+$, when CO is depleted from gas-phase. For diazenylium (N_2H^+) they found that its ^{15}N fractionation follows that of molecular nitrogen since N_2H^+ is mainly produced by $H_3^+ + N_2$ and destroyed by CO back to N_2. When CO depleted from gas-phase (after about 10^4 yr), N_2 is more important in the destruction of $^{15}NNH^+$,

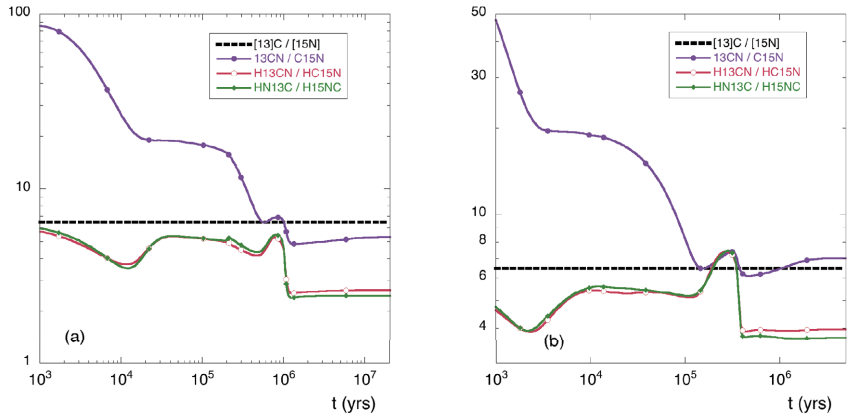

Fig. 1.20: Time evolution of $^{13}C/^{15}N$ ratios of CN, HCN, and HNC for models (a) and (b), found by Roueff et al. (2015). The $^{13}C/^{15}N$ elemental ratio is displayed as a dotted line. Taken from Roueff et al. (2015).

converting it into N_2H^+ and increasing the $N_2H^+/^{15}NNH^+$ ratio. $N^{15}NH^+$ follows a similar trend but, due to reactions (1) and (2), it has a larger enhancement in ^{15}N with respect to $^{15}NNH^+$. However, the higher $^{14}N/^{15}N$ ratios of $^{15}NNH^+$ with respect to the nominal value of 220 are far from the very depleted ratio observed in L1544 by Bizzocchi et al. (2013).

- Then, they updated the chemistry used by Wirström et al. (2012) with the new nitrogen chemistry given by KIDA database. With this new complete model they found the results shown in Fig. 1.23, that two orders of magnitude less CN is maintained in the gas phase of a dense core. Thus, since nitriles are mainly enhanced in ^{15}N from reactions with CN, as discussed above, this low CN abundance suppresses the ^{15}N fractionation in HCN and HNC. The reason why CN is so under abundant with respect to the old model (Wirström et al. 2012) is the reaction 1.42, that previously had a zero reaction rate. Moreover, in this updated network the effects on the ^{15}N fractionation of N_2H^+ and ammonia are unchanged.

As a conclusion, Wirström and Charnley (2018) also pointed out that the barriers of reactions (7), (8) and (10) were evaluated based on a linear geometry, and other approach angles on the potential energy surface might allow the reaction to proceed. So, laboratory studies are needed to confirm or not the presence of these barriers.

Loison et al. (2019): Up to 2018, no astrochemical model based on gas-

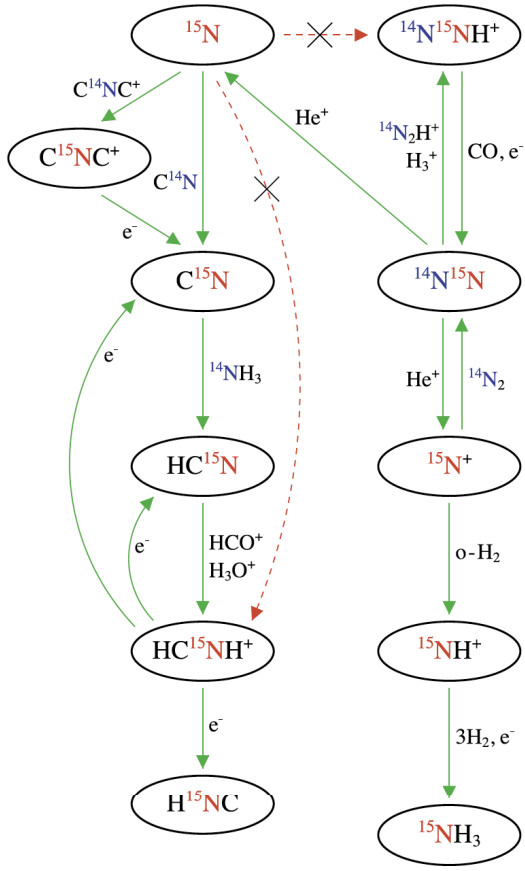

Fig. 1.21: Revised chemical network illustrating the main reactions that causes ^{15}N fractionation in nitrile-bearing species and amines. Red dashed arrows indicate reactions that are ineffective according to Roueff et al. (2015). The lines stop when the molecule freeze-out on grains. Taken from Wirström and Charnley (2018).

phase chemistry alone has been able to produce nitrogen fractionation levels greater than a few per cents. Moreover, since Wirström and Charnley (2018) included only simplified grain processes such as the depletion of gas-phase species onto grains, Loison et al. (2019) developed a new chemical model with also grain surface chemistry and grain desorption. They considered also cosmic-ray induced photodissociations, and introduced new ^{15}N exchange reactions (see Table 1.2). In this work they assumed that all the isotopic-exchange reactions involve adduct formation, which corresponds to the reactions of type B described above.

They assumed a n_{H_2}=2×10^4 cm^{-3}, a gas and dust temperature of 10 K,

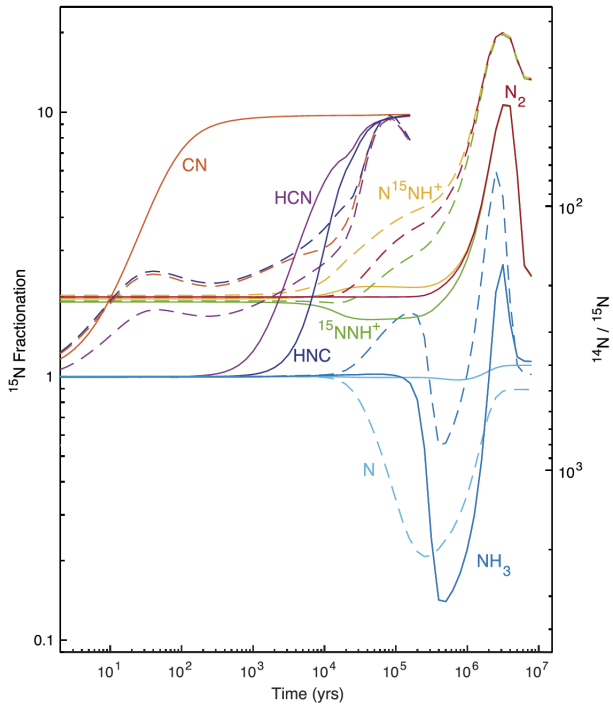

Fig. 1.22: Time dependence of $^{14}N/^{15}N$ isotopic ratios of the major nitrogen-bearing gas-phase species, as predicted by Wirström et al. (2012) (dashed lines) and the updated model by Wirström and Charnley (2018) with the new rate for isotopic exchange reactions given by Roueff et al. (2015) (solid lines). The lines stop when the molecule freeze-out on grains. Taken from Wirström and Charnley (2018).

a cosmic-ray ionisation rate of 1.3 $\times 10^{-17}$ s^{-1} and a total visual extinction (A_V) equal to 10. They investigated reaction (23) of Table 1.2, but since the two exothermic channels form HCN and $HC^{15}N$ with the same rate, then, this reaction is not efficient to fractionate. Moreover, they did not take into account the isotopic-exchange reaction between ^{15}N and CN since the exit channel that gives rise to C + ^{15}NN is the most important one (reaction (21) of Table 1.2; Daranlot et al. 2012).

Their model leads to low fractionation level but with some interesting results:

- As can be noted from Fig. 1.24, it was found a lower $^{14}N/^{15}N$ for HNC because of reaction (24) that is more efficient in creating $H^{15}NC$ than $HC^{15}N$.
- Another important result is given by the mass dependence on the accretion time on grain surfaces for different isotopologues. In fact, ^{14}N will

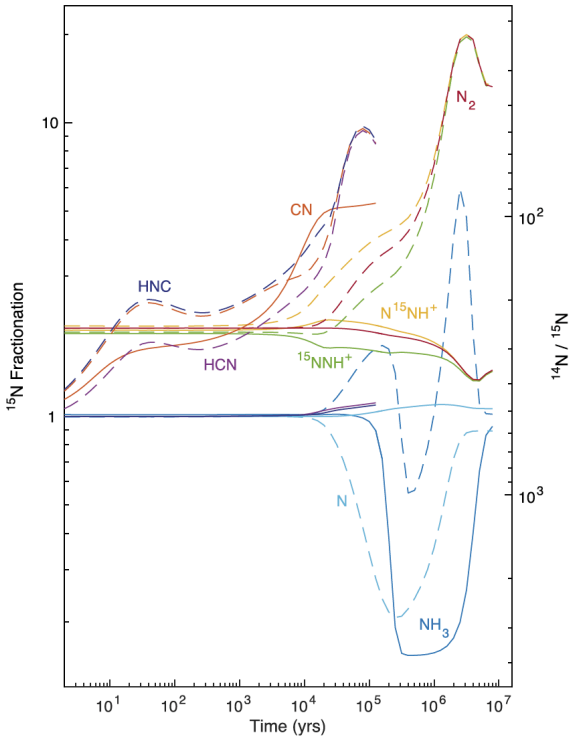

Fig. 1.23: Time dependence of $^{14}N/^{15}N$ isotopic ratios in the major nitrogen-bearing species in gas-phase, as predicted by Wirström et al. (2012) (dashed) and the updated model by Wirström and Charnley (2018) with the new rate for isotopic exchange reactions given by Roueff et al. (2015) and the nitrogen reaction rates based on Wakelam et al. (2013) (solid lines). Taken from Wirström and Charnley (2018).

be removed from the gas phase more quickly than ^{15}N. As a consequence, for most of the species the $^{14}N/^{15}N$ is around 400 (slightly lower than the initial condition of 440). However, this process is not efficient for evolved clouds because desorption mechanisms will release ^{14}N-bearing molecules back into the gas phase. Loison et al. (2019) found values, at time scales around (3–6)$\times10^5$ yr, that are still above the typically observed values for different molecular species (e.g. Daniel et al. 2013) or still lower than the observed values for N_2H^+ in pre-stellar cores (e.g. Bizzocchi et al. 2013). Using an initial $^{14}N/^{15}N$ of 300 (e.g. Romano et al. 2017) they found results in agreement with most of the observations of CN, HCN, HNC and ammonia (red dotted lines of Fig. 1.24).

- Finally, they discussed what mechanism could enhance the ^{15}N in N_2H^+. Reactions (1) and (2) of Table 1.1 are inefficient due to their low exother-

Table 1.2: New reactions introduced in the model of Loison et al. (2019).

Label	Reaction	k_f ($cm^3\ s^{-1}$)	$f(B,m)$	ΔE (K)
(21)	$^{15}N + CN \rightleftharpoons C + {}^{15}NN$	$8.8\times10^{-11} \times (\frac{T}{300})^{0.42}$	–	–
	$^{15}N + CN \rightleftharpoons N + C^{15}N$	0	–	–
(22)	$NH_4^+ + {}^{15}NH_3 \rightleftharpoons {}^{15}NH_4^+ + NH_3$	$1.3\times10^{-09} \times (\frac{T}{300})^{-0.5}\times$ $\times \frac{1}{1+\exp(-14.5/T)}$	1	14.5
(23)	$HCNH^+ + H^{15}NC \rightleftharpoons HC^{15}NH^+ + HCN$	$1.0\times10^{-09} \times (\frac{T}{300})^{-0.5}$	–	0
	$HCNH^+ + H^{15}NC \rightleftharpoons HCNH^+ + HC^{15}N$	$1.0\times10^{-09} \times (\frac{T}{300})^{-0.5}$	–	0
(24)	$HC^{15}NH^+ + e^- \rightleftharpoons HC^{15}N + H$	$9.34\times10^{-08} \times (\frac{T}{300})^{-0.64}$	–	0
	$HC^{15}NH^+ + e^- \rightleftharpoons H^{15}NC + H$	$9.90\times10^{-08} \times (\frac{T}{300})^{-0.64}$	–	0

micity. Taking into account the chemistry of N_2H^+, it is mainly driven by three reactions:

$$N_2 + H_3^+ \rightarrow H_2 + N_2H^+, \tag{1.44}$$

$$N_2H^+ + e^- \rightarrow N_2 + H, \tag{1.45}$$

$$N_2H^+ + CO \rightarrow N_2 + HCO^+. \tag{1.46}$$

Reactions (1.44) and (1.46) are barrierless and then their rate coefficient is not affected by the ZPE difference of any of the N_2H^+ isotopologues. Moreover, they assumed in their model that the rate coefficient for (1.45) for all the isotopologue is the same. However, Lawson et al. (2011) showed experimentally that this could have differences of about 20% between 300 and 500 K, being the reaction for N_2H^+ more efficient than that of $^{15}N_2H^+$ and N_2D^+. So they assumed that, due to the difference in ZPE of the ^{15}N-isotopologues, there is an increase at low temperature for the rate coefficient of $^{15}NNH^+$ and $N^{15}NH^+$. As a consequence, the $N_2H^+/{}^{15}NNH^+$ and the $N_2H^+/N^{15}NH^+$ ratios will increase above the initial nitrogen isotope ratio value given in the model. In particular, as shown in Fig. 1.25, they found $^{14}N/^{15}N$ around 900 at the age of the typically observed clouds, and when CO depletion is more inefficient, the $^{14}N/^{15}N$ ratio becomes about 600.

In summary, all this demonstrates that current chemical models cannot reproduce observed variation in nitrogen fractionation, and then a lot of work remains to be done to clarify, from a theoretical point of view, the nitrogen fractionation issue from diffuse clouds to the Solar system.

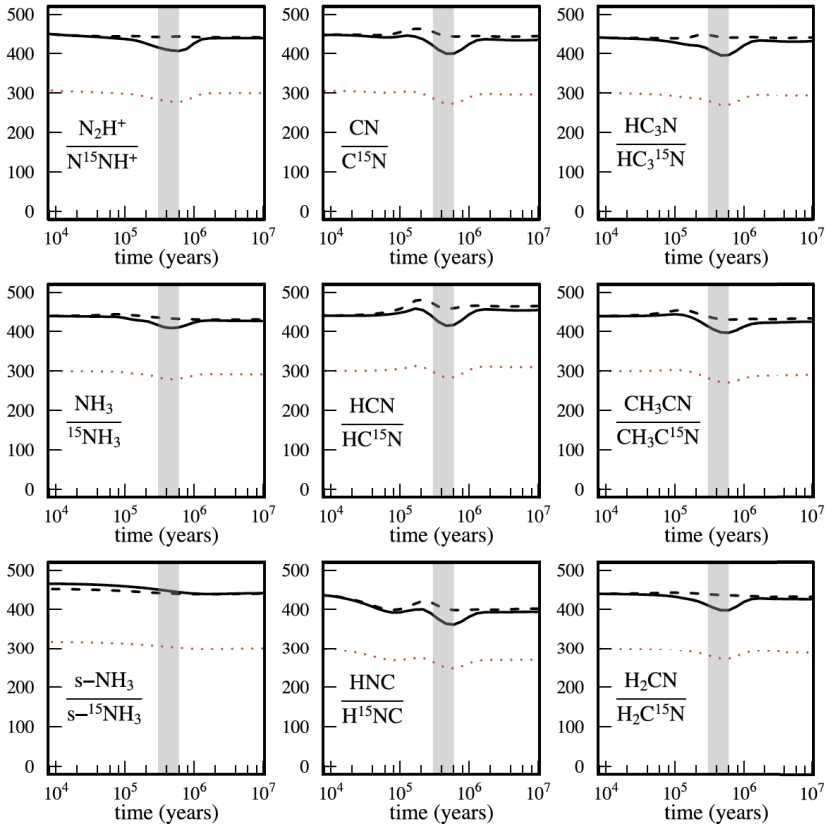

Fig. 1.24: Time dependence of the $^{14}N/^{15}N$ for the main nitrogen species in the gas phase, for an elemental $^{14}N/^{15}N$ of 441 (continuous black lines), and equal to 300 (red dotted lines), obtained by Loison et al. (2019). The black dashed lines represent the model with the same sticking rate coefficient for all isotopologues of a given species. The vertical grey rectangle represents the TMC-1 cloud age.

The first results towards high-mass star-forming regions

The results shown so far indicate that it is important to gather more data to put stringent constraints on current chemical models. Moreover, as already done for D-fractionation, it is important to investigate the possible link between cometary and ISM material in intermediate- and high-mass star-forming regions, since there is growing evidence that our Sun was born in a rich stellar cluster (see Sect. 1.2). Thus, measurements of the $^{14}N/^{15}N$ ratio in high-mass star-forming regions could provide insight into the initial bulk composition of the PSN.

One of the first samples of high-mass star-forming regions was observed by

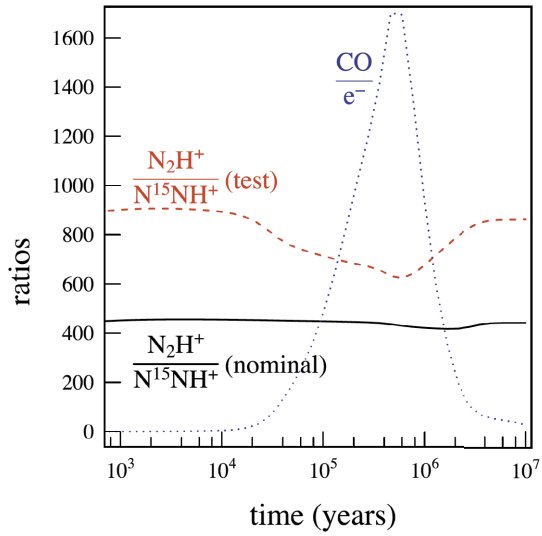

Fig. 1.25: Time dependence of the $N_2H^+/N^{15}NH^+$ ratio for the nominal model (black solid line) and for a N_2H^+ dissociative recombination rate divided by 2 (dashed red line). The dotted blue line corresponds to the CO/e^- ratio. Taken from Loison et al. (2019).

Adande and Ziurys (2012). They measured the $^{14}N/^{15}N$ ratios from CN, and HNC, and found values between ∼194 and ∼391. For CN they found a range of values from ∼122 up to ∼361 and for HNC from ∼134 up to ∼406. The main goal of their work was to derive the $^{14}N/^{15}N$ ratio as a function of the Galactocentric distance (D_{GC}). The importance of this behaviour and its link with the prediction of Galactic chemical evolution models will be discussed in chapter 3.

Fontani et al. (2015b) continued this observational investigation deriving the $^{14}N/^{15}N$ ratio for N_2H^+ in the same sample of sources studied in Fontani et al. (2011). The $^{14}N/^{15}N$ ratios that they found show a large spread of values, from ∼180 up to ∼1300. They were also able to derive the N-fractionation from CN in 13 of the sources of the total sample, finding $^{14}N/^{15}N$ in between ∼190 and ∼450. These values are consistent, within the errors, with both the TA value (270) and the PSN value (441). An important conclusion of their work is the non-correlation of the $^{14}N/^{15}N$ ratios with the evolutionary stage of the sources, which, differently for the D/H ratio, indicates that time is irrelevant for the fractionation of nitrogen. Moreover, they found the first hints of a possible anticorrelation between H/D and $^{14}N/^{15}N$ ratios, in agreement with the prediction of Wirström et al. (2012). The possible link between the two isotopic ratios will be discussed in more detail in chapter 2.

Later, Zeng et al. (2017) observed a sample of 22 cold and dense cores

at the initial stages of their evolution (IRDCs), which are believed to be the precursors of high-mass stars and star clusters. These regions present physical conditions that resemble those of the early stages of the Solar system formation. Towards this sample Zeng et al. (2017) found $^{14}N/^{15}N$ ratios between ∼70 and ∼458 for HCN (excluding the lower limits), and between ∼161 and ∼541 for HNC. The IRDCs that they observed towards G034.77-00.55 (cloud G) show lower nitrogen isotopic ratios than the other clouds. One possible explanation is the lower mass surface densities that they present (∼0.4 g cm^{-2}) and also the fact that they are in an earlier stage of evolution. The authors proposed that, instead of temperature, the gas density may be the predominant parameter influencing the $^{14}N/^{15}N$ in the young PSN.

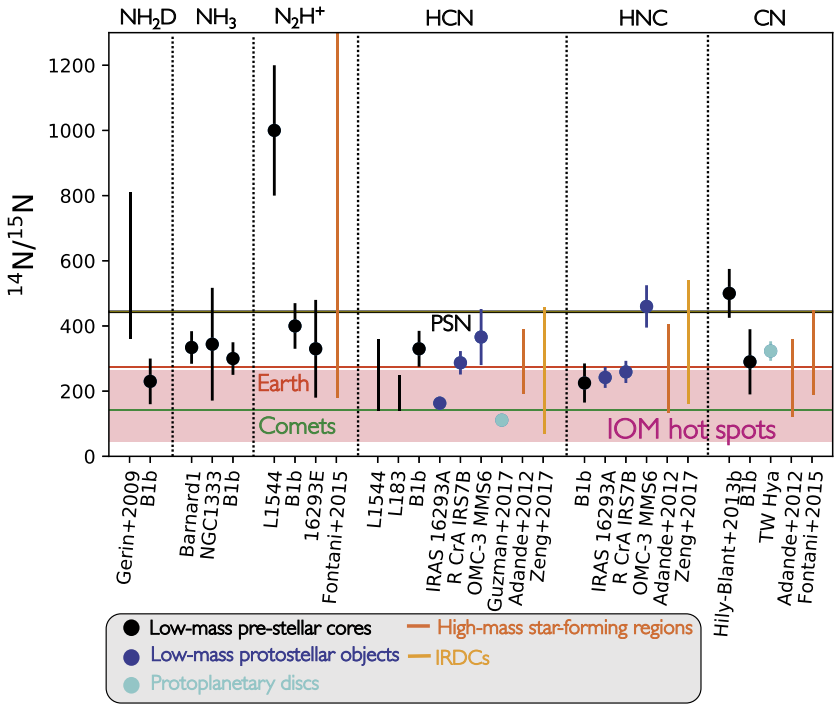

Fig. 1.26: The same as Fig. 1.16. Moreover, light orange ranges represent the IRDCs, and the dark orange indicate high-mass star-forming regions.

Updating the Fig. 1.16 with the results towards high-mass star-forming regions, Fig. 1.26 is obtained. Even towards these sources there are hints of differences between protonated molecules (N_2H^+) and nitrile-bearing species. However, the number of sources is still low, and a direct comparison between different molecules in the same sample of sources is still missing. Indeed, this is exactly the starting point of this thesis that will be presented in detail in

next chapters.

1.5. Thesis project

The mechanisms leading to enrichments of the less abundant isotopes of elements in molecules in different phases of star-formation are still not well known. In this introduction we have presented the state-of-the-art of the observational results in low- and high-mass star-forming regions, and the comparison between H- and N-fractionation, which shows the largest anomalies in pristine Solar system material. Moreover, we have presented the history of chemical models that tried (and still try) to interpret these results, and give an answer to these anomalous isotopic enrichments. We have also shown the relevance of studying the environment where massive stars are born, since nowadays there is a growing evidence that our Sun was born in a rich cluster, containing also massive stars.

The main goals of this thesis are summarised as follows:

- To study the N-fractionation of HCN and HNC in the same sample of high-mass star-forming regions in which Fontani et al. (2011) analysed N_2H^+ and compare H- and N-fractionation in this sample.

- To study the behaviour of the $^{14}N/^{15}N$ ratio as a function of the Galactocentric distance in a large sample of high-mass star forming regions (87 sources); and compare with the Galactic Chemical Evolution models of Romano et al. (2017) and Romano et al. (2019).

- To zoom into one of the sources of the sample (IRAS 05358+3543) with interferometric observations, studying the morphology of ^{15}N-enrichments in N_2H^+ at linear scales capable to resolve different substructures of the source.

- To develop a gas-grain chemical model to study in detail the behaviour of $^{12}C/^{13}C$ of nitrile-bearing species in different types of star-forming regions and how this can influence the calculation of the N-fractionation that starts from ^{13}C-bearing species.

This thesis is organised as follows:

- In chapter 2 and 3 I present the study of a sample of high-mass star-forming regions with single-dish observations in order to give statistically significant results both on the comparison between H- and N-fractionation and on the Galactic chemical evolution of the $^{14}N/^{15}N$.

- In chapter 4 I present an interferometric study of the source IRAS 05358+3543 to investigate how the $^{14}N/^{15}N$ of N_2H^+ changes towards an entire high-mass star-forming region on scales of a few arcseconds.

- Finally, in chapter 5 I present a chemical model to study the $^{12}C/^{13}C$ ratio for nitrile-bearing species and to estimate the error made in evaluating the $^{14}N/^{15}N$ ratio assuming a fixed $^{12}C/^{13}C$ that only depends on the Galactocentric distance.
- In chapter 6 I summarise the main conclusions of this thesis.